ULTRASONIC CHARACTERIZATION OF KENYAN CLAY REFRACTORIES

BY

FRANCIS WANJALA NYONGESA
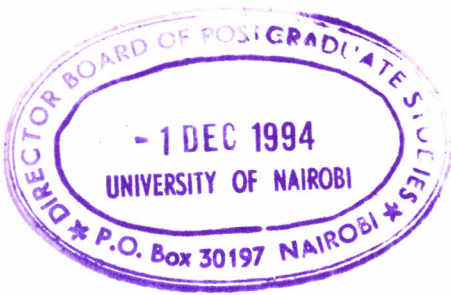
Thesis submitted in partial fulfilment for the degree of Master of Science of the University of Nairobi.

MARCH   1994

DECLARATION

This thesis is my original work and has not been presented for a degree in any other University.

FRANCIS WANJALA NYONGESA
University of Nairobi

This thesis has been submitted for examination with the approval of my University supervisors

Dr. B. ADUDA
Department of Physics
University of Nairobi

Dr. E. SARHENE
Department of Physics
University of Nairobi

ABSTRACT

Characterization of ceramic materials is important in order to improve their quality. In this study ultrasonic nondestructive technique has been used to characterize some Kenyan clay refractories. Ultrasonic parameters used for characterization were velocity and frequency dependent attenuation measurements. It was found that the ultrasonic parameters are influenced by the material fabrication conditions.

The measured ultrasonic velocity in the clay refractories was found to increase as the firing temperature and/or the compaction (loading) pressure were increased. Meanwhile the ultrasonic attenuation decreased with increase in the firing temperature and/or the compaction pressure. Further, clay refractories fabricated from different types of clay, (*red firing clay* -RFC and *red hill clay* -RHC) gave different velocity and attenuation values. Ultrasonic velocity in refractories fabricated from the clays with a `finer´ particle size distribution (RFC) was higher than that in refractories fabricated from clays with a `coarser´ particle size distribution (RHC).

The material properties such as bulk density and shrinkage (both linear drying shrinkage -$\%LDS_f$ and linear firing shrinkage -$\%LFS_d$) were also found to increase with increasing firing temperature or loading pressure. Further, high shrinkage values were noted in samples with a `finer´ particle size distribution (RFC).

X-ray diffraction (XRD) and chemical (rational) analysis showed that the proportions of most of the major clay minerals (such as quartz, mica and feldspar) increased as firing temperature was increased. The proportion of kaolinite however dropped with temperature.

ACKNOWLEDGEMENT

TABLE OF CONTENTS

LIST OF SYMBOLS

A   Cross sectional area

A_n Amplitude of sound waves

D   Transducer diameter

d   Sample thickness

$\mathbb{D}$ Average grain size

E   Young's modulus

$E(p)$ Young's modulus at porosity p

E_o Young's modulus at zero porosity

f Frequency of sound waves

G   Shear modulus of elasticity

I_o Intensity of incident ultrasonic wave

I_x Intensity of ultrasonic wave at distance x

jX   Reactive sound propagation term attributed to inertia and stiffness of the medium

K   Bulk modulus of elasticity

% LDS_f Linear drying shrinkage on the formed basis

% LFS_d Linear firing shrinkage on the dried basis

L_d Dimension of dried unfired sample

L_f Sample forming dimension

L_F Sample fired dimension

M   Ratio of characteristic impedance of two media

NF   Near field distance

NDE   Nondestructive evaluation

p porosity

p_T Total porosity

RFC   Red firing clay

RHC   Red hill clay

R   Reflection coefficient

(v)

R_{ac} Acoustic resistance

S Strength of brittle polycrystalline solids

S Cross sectional area

Θ_1 Angle of incidence

Θ_2 Angle of refraction

T Transmission coefficient

t Transit time

V Velocity of sound waves

V_i Velocity of sound waves in medium i

V_l compressional velocity

V_r Rayleigh or surface wave velocity

V_s Shear wave velocity

Z_{ac} Acoustic impedance

Z_i Acoustic impedance of medium i

Z_{sp} Specific acoustic impedence

α Attenuation coefficient

α_a Absorption coefficient

α_s Scattering coefficient

λ Wavelength of sound waves

σ Poisson's ratio

ρ Specimen bulk density

ρ_i Bulk density of medium i

ρ_t True bulk density of a sample

ω First critical angle

LIST OF TABLES

LIST OF FIGURES

CHAPTER ONE

INTRODUCTION

1.1 Introduction

Clays form a class of traditional ceramics. This class of ceramics include also materials such as cements and silicate glasses [Kingery, 1975]. In Kenya's ceramic industry, local clays are the principal raw materials. The manufacture of most ceramic products such as sanitary ware and refractory products (fire clay bricks and thermal insulation bricks), is based mainly on clays. Furthermore, the art of forming and burning of clays has been in practice for many decades in this country.

The principal clays used in Kenya's ceramic industry include; Red firing clay, Red hill clay and Ball clay. Red hill clay is obtained from volcano ashes. This clay has a high thermal stability and is a good candidate for furnace linings. Red firing clay, as the name suggests becomes red in colour when fired and it is the most locally available clay. Red firing clay has found wide application in manufacture of refractory products; thermal insulation bricks, fire clay bricks and in pottery. Ball clay is a white plastic clay which, in Kenya, is found mostly within coastal regions and around river banks. This clay is an essential ingredient for ceramic body manufacture as binding agents for imparting plasticity, workability and green strength to raw materials [Kshama *et al*, 1992]. However, in most cases, it is rare that any clay can be found which satisfies all the manufacturing requirements of any one product [Kshama *et al*, 1992; Veniale *et al*, 1992; Abdel-aziz *et al*. 1991]. For this reason, blended clays are produced consisting of

1

many components from several individual seams each contributing to the physical properties of the final blend.

Despite the wide use of clays in the Kenyan ceramic industry, the properties of these clays as well as the clay products have not been well characterized as compared to most modern ceramics (such as borides, carbides, nitrides, single and mixed oxides, silicates etc.). The lack of characterization of local clays has led to poor quality and unreliable local ceramic products. Characterization of local clays would not only improve the performance of these materials but widen their application in the ceramic industry as well.

1.2 Statement of the Problem

The problem of poor quality of most local refractory products, for example, the low mechanical strength of fire clay bricks could be solved by proper control of fabrication conditions and controlling of the microstructure of the materials.

Scientific studies have shown that the strength of most ceramic materials is dependent on fabricating (processing) conditions. For example, Ibisi, (1991) has shown that increase in firing temperature increases the density, percentage shrinkage and the modulus of rupture in some Nigerian clays. Klima *et al*, (1987) showed that the loading pressure and firing temperature determine the density and microstructure in sintered ceramics of silicon carbide and nitride. The packing of grain in a sample during compaction has been shown to be influenced mostly by the compaction and distribution of particle sizes [Kshama *et al*, 1992]. However, in our local ceramics, little or no scientific study has been carried out to assess the effect of

processing conditions on the strength of ceramic materials. Investigation of the effects of fabrication parameters on the material properties such as density and elastic moduli of the final product is hence vital.

Further, in order to improve the quality and reliability of our local ceramic products, it is necessary to gain insight into the material properties by controlling their microstructure. This is possible on the basis of ultrasonic parameters if the investigation of the effect of fabrication parameters on the material properties of a final ceramic product is possible through the ultrasonic nondestructive evaluation (NDE) method.

1.3 Objectives of the Present Study

The primary objective of this study is to investigate using the ultrasonic nondestructive evaluation (NDE) technique, the effect of processing conditions such as compaction pressure, firing temperature and particle size distribution on the material properties of the final refractory clay products. Samples of Red firing clay and Red hill clay hereafter designated RFC and RHC respectively were chosen for this study. Variations in the material properties such as density, ultrasonic velocity and hence Young's modulus (E), and ultrasonic attenuation were determined nondestructively via interaction of sound waves with the microstructure and morphological factors (i.e. particle size and shape) of the material. Changes in the mineralogical composition developed in the samples on firing were determined by Rational analysis and X-Ray diffraction studies (XRD). Further, the sample's microstructure were determined through observing thin sample sections under optical microscope.

The aims of the present study are fourfold:

(i) To study the effect of different fabricating or processing conditions i.e. particle size distribution, compaction pressure and firing temperature on the materials properties such as bulk density and Young's modulus.

(ii) To investigate the effect of material microstructure and morphology (particle size and shape), on the speed of wave propagation (velocity) and wave energy loss (attenuation)

(iii) To correlate the two ultrasonic parameters i.e. (velocity and attenuation) with the material's bulk density and Young's modulus

(iv) Estimate the Elastic constant (E) from velocity measurements.

The samples used were processed at various conditions; The compaction (loading) pressure ranged from 64 MPa to 255 MPa, While the firing temperature ranged from 600° c to 950° c.

CHAPTER   TWO

REVIEW OF ULTRASONIC (NDE) TECHNIQUE   FOR CERAMIC MATERIALS

2.1. Characterization of Microstructure

Many studies have dealt with   the application   of   ultrasonic

testing to characterize and monitor the properties   of ceramic

materials nondestructively [Klima *et al*, 1987; Gieske *et al*, 1991;

Gault, 1989; Kupperman *et al*, 1984; Kreher, 1977].

The principle of ultrasonic material characterization is based on the

measurement of the velocity of sound waves and the loss of wave energy

when the ultrasonic wave traverses the material under test and

frequency analysis. Klima *et al*, (1987) have   used the ultrasonic

parameters (velocity and attenuation measurements) for density and

microstructure   characterization in sintered silicon carbide and

nitride. They reported an increase in ultrasonic velocity with density

in these ceramics as shown in fig 2.1. Kupperman *et al*, (1984) also

reported a similar trend in the variation of ultrasonic velocity with

density in green MgO.
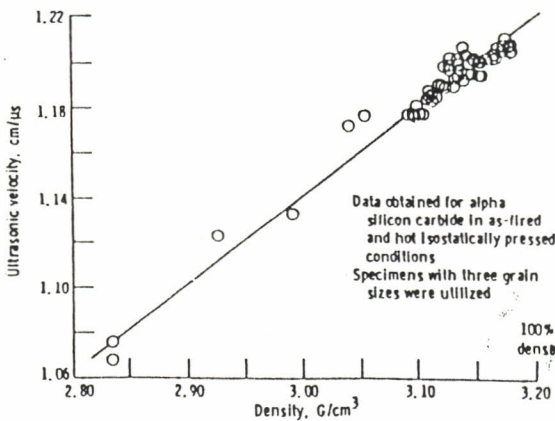
Fig. 2.1. – Ultrasonic velocity as a function of bulk
density for alpha silicon carbide (Klima *et al*. 1987).

5

Kreher *et al.* (1977) measured ultrasonic velocity in electrical porcelain bodies fabricated in varying mass of K_2O/ SiO_2/ Al_2O_3 as a function of porosity and pore shape at different firing temperatures. They assumed uniform elastic properties and non spherical pores in the medium and showed that there exists a minimum porosity, obtained at an optimal firing temperature, for which the maximum ultrasonic velocity was obtained. The results obtained by Kreher *et al,* (1977), for some of the compositions are shown in figures 2.2 and 2.3. In these figures the general variation of porosity and ultrasonic longitudinal velocity related to the firing temperature for different compositions of electrical porcelain are shown.
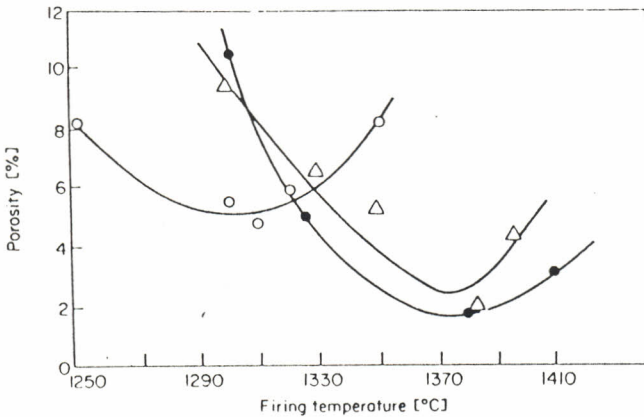
Fig. 2.2. -Curves of the porosity versus firing
temperature (Kreher et al, 1977).

6
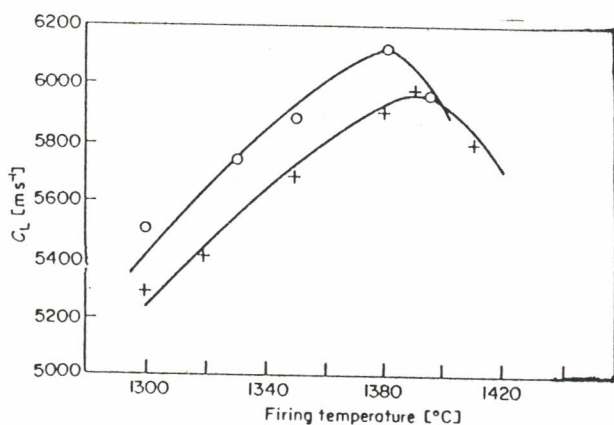
Fig. 2.3. -Ultrasonic wave velocity as a function of firing temperature (Kreher, 1977).

The material microstructure is known to influence the propagation of ultrasonic parameters in the material [Vary, 1988]. As most material properties such as density, and Young's modulus, and microstructure are determined by fabricating conditions, it is no doubt that the ultrasonic parameters will be dependent on sample fabricating conditions. For example increase in firing temperature has been shown to increase (though non linearly) the density, percentage shrinkage and the modulus of rupture in some four Nigerian clays designated MPP, KAP, KWP and AFP as shown in figures 2.4a and 2.4b [Ibisi, 1991].

7
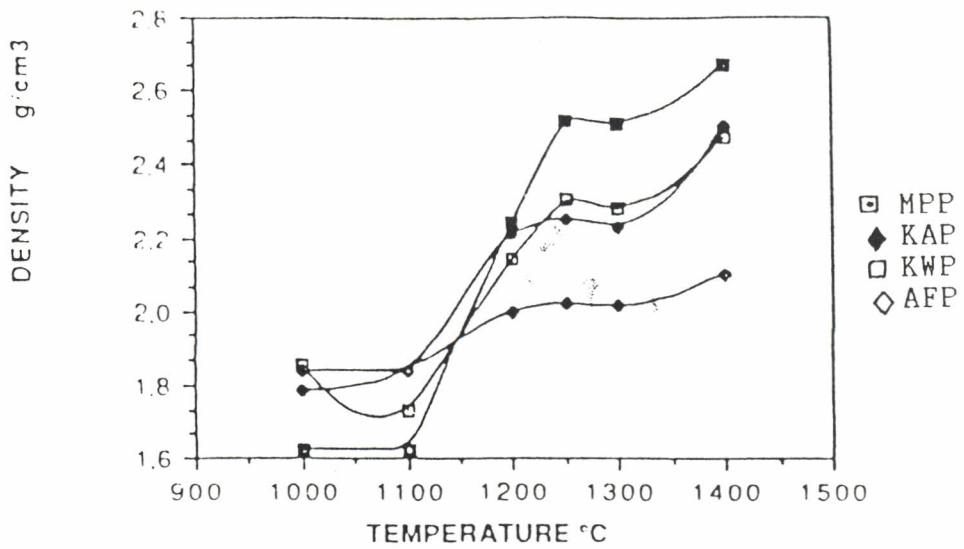
Fig. 2.4a. -Variation of bulk density with temperature for some Nigerian clay samples (Ibisi, 1991).
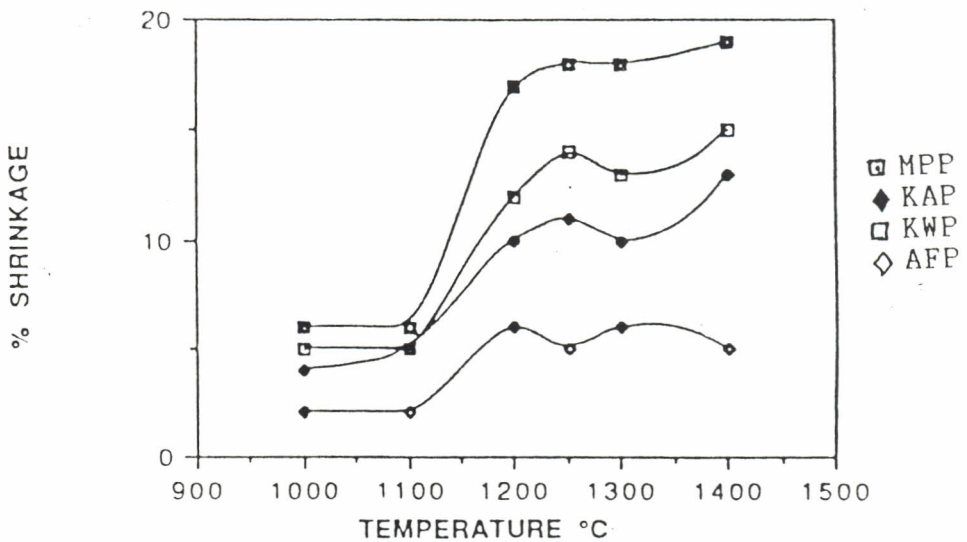
Fig. 2.4b. -The percentage shrinkage of some Nigerian clay samples as a function of temperature (Ibisi, 1991).

Kobayashi *et al.* (1992) has reported an initial increase in bulk density in three porcelain bodies A, B and C with increasing firing temperature as shown in Fig 2.5. Bodies A and B had quartz, feldspar and kaolinite as their main constituents while boby C was composed of sericite, kaolinite and large amounts of quartz. According to Kobayashi *et al.* further temperature increase, beyond T_d causes the bulk density to drop from its maximum value which was observed at temperature T_d. The variation of apparent porosity with firing temperature in these materials was observed to be an inverse to the bulk density results.
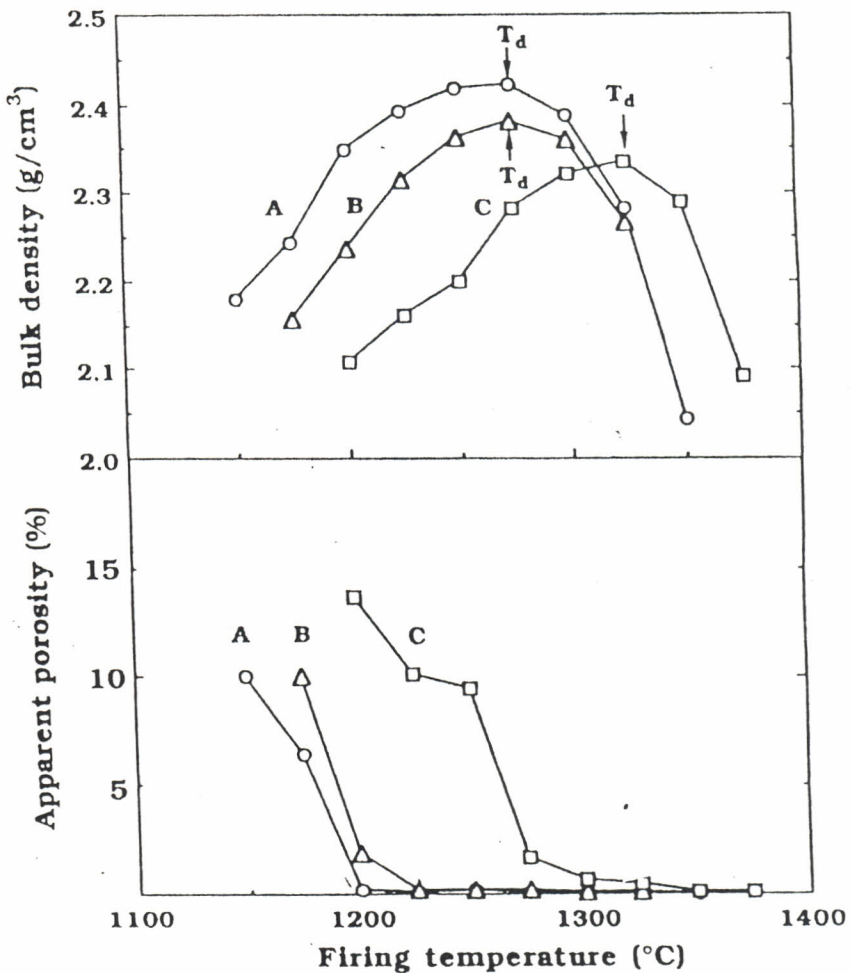
Fig. 2.5. —The effect of firing temperature on bulk densit and apparent porosity in porcelain bodies (Kobayashi *et al* 1992).

Klima *et al*, (1987), have shown that the loading pressure (compaction pressure) and firing temperature influence the density and microstructure of sintered ceramics (silicon carbide and silicon nitride). Further, Klima *et al*, observed that sintered materials with a fine microstructure were significantly stronger at room temperature than the materials with coarser microstructure. Figure 2.6 shows an example of a fine and coarse microstructure.
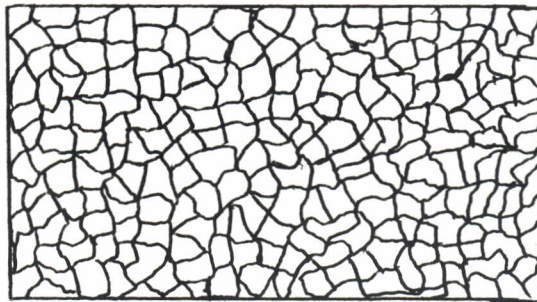
a. fine microstructure
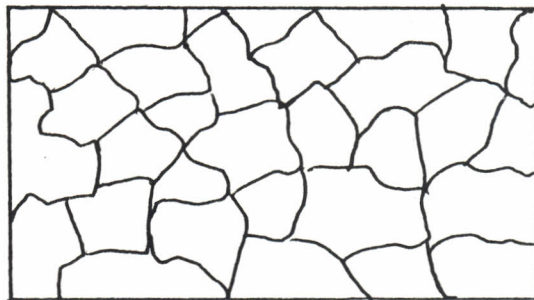
b. coarse microstructure

Fig. 2.6. -An illustration of 'fine' and 'coarse' microstructure

The packing of particles in a ceramic sample during compaction has been shown to be influenced mostly by the degree of compaction and distribution of particle sizes [Kshama *et al*, 1992]. The ultrasonic parameters are therefore dependent on material processing conditions.

One of the methods for assessing microstructure is that of measuring attenuation caused by the grain structure of polycrystalline solids [Vary, 1988]. Variations in microstructural features such as grain size or shape, have been found to have a pronounced effect on ultrasonic attenuation [Klima et al, 1987; Vary, 1988; Gault, 1989]. High ultrasonic attenuation have been reported in inhomogeneous materials such as biological materials-human tissues [Wear. et al, 1993], concrete [Gaydecki et al, 1991; Lefebvre et al, 1980], composite materials, and sea bed sediments [Chivers, 1991]. Klima et al, (1987) found that attenuation in large grained materials of sintered ceramics was much more than the attenuation in the small grained materials as shown in figure 2.7 below.
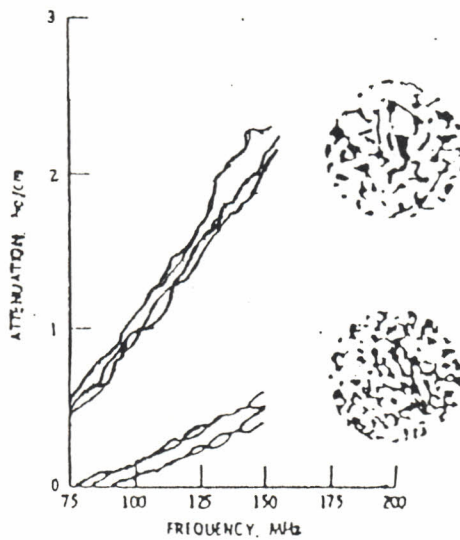
Fig. 2.7. -Effect of microstructure on attenuation in sintered silicon carbide (Klima et al, 1987).

11

Evans *et al*, 1977, have quantitatively shown that attenuation in a porous reaction-bonded Si_3N_4 derives primarily from a narrow range of grain (pore) sizes. Further theoretical analysis of the effects of grain size distribution in polycrystalline materials on the frequency dependence of the ultrasonic attenuation has been presented by Smith, (1982). Smith has shown that two specimens with the same mean grain diameter can have significantly different ultrasonic attenuations if their grain size distributions are different.

In green ceramics, conventional ultrasonic techniques are usually difficult to apply for sample characterization because of the high attenuation in these specimens, fragility and the couplant-absorbing properties of these materials [Kupperman *et al*, 1984]. However, Kupperman *et al* 1984; Jones *et al*, 1986, have studied and assessed the effectiveness of ultrasonic methods in green (unfired) ceramics by pressure coupled transducers and dry coupling (via elastomers) respectively. In these studies it was found possible to relate pertinent material properties such as the moduli of sintered ceramics to their green-state elasticity. Accordingly, such studies could lead to rejection of ceramics possessing poor green-state elastic properties and thereby avoiding further costly processing.

It is generally recognized that the strength of a specimen is dependent on its porosity and grain size. Knudsen *et al*, (1959) proposed a formula relating the variation in strength S of porous brittle polycrystalline specimens with changing porosity (p) and grain size (D) that has proved to be valid for various

types of strength tests; compression, tension or bending etc. This
expression is written as

$$S = K_1 D^{-a} e^{-bp} \quad \dots\dots\dots\dots\dots\dots\dots\dots\dots\dots(2.1)$$

where a, b, and K_1 are empirical constants. Further, Knudsen showed
that variations in the degree to which specimens were fired
appeared to have an effect on the final specimen strength
exclusive of the strength attributable to the resultant changes in
porosity and grain size.

2.2. Elastic moduli

The measurement of elastic moduli is fundamental to understanding and
predicting material behavior. Because they are related to interatomic
forces, elastic moduli govern attainable strengths. Elastic moduli
also govern the strain energy release rate and the stress wave
propagation properties associated with shock, impact, fracture, etc.
[Vary, 1988]. Ceramic materials generally require ultrasonic velocity
measurements to evaluate elastic moduli since tensile tests produce
either poor or no results. Further, moduli of ceramics are easier to
determine ultrasonically since they exhibit very small strains under
tension [Vary, 1988]

Many studies have dealt with the application of ultrasonic velocity
measurements to determine the elastic moduli in ceramic materials.
For example Klima et al, 1987, reported an exponential variation of
Young's modulus E with increasing density, which in terms of porosity
(p) is written as

$$E = E_o \exp^{-bp}. \qquad \dots\dots\dots\dots\dots\dots\dots(2.2)$$

where E_o is Young's modulus at zero porosity and b is a constant. Nagarajan, (1970), deduced a quadratic relation for the dependence of Young's and shear moduli on porosity. Kreher *et al*, (1970), demonstrated relations among transverse and longitudinal velocities and elastic moduli of porous ceramics. Fanzy *et al*, (1985), have reported a mathematical correlation between the ultrasonic velocity and the dynamic modulus of elasticity in five fired refractory products (high alumina, super-duty fireclay, vitreous silica and carbon). Further, Fanzy *et al*, confirmed the usefulness of the modulus of elasticity measurements to generate valid strength estimates for a variety of refractory products.

Kathrina *et al*, (1991), have monitored the setting process of phosphate-bonded, alumina-filled, magnesia ceramics using ultrasonic double-probe method in samples with alumina content in the range 0- 60% weight. The elastic properties determined from ultrasonic velocity measurements were found to be dependent upon the filler volume fraction, while the reaction rate was found to increase with increasing overall filler volume fraction According to Kathrina *et al*, (1991), the measured elastic moduli increased exponentially with decreasing porosity. Panakkal, (1991) has compared the reported values of elastic moduli of uranium dioxide and ultrasonic velocity in these materials for different pore volume fractions. He has shown that longitudinal velocity may be used as a predictor of elastic modulus of sintered uranium dioxide without measuring density.

14

Phani *et al*, (1986) developed an expression relating Young's modulus (E) to porosity (*p*) for four gypsum systems. This relation was found applicable over the entire range of porosity (*p*). Phani *et al*'s expression is of the form

$$E = E_o(1 - ap)^n, \quad \dots\dots\dots\dots\dots\dots\dots\dots(2.3)$$

where E_o is the Young's modulus at zero porosity, n is a material constant, while a is the packing geometry. In the derivation of equation 2.3, Phani *et el*, (1986), assumed that the physical process such as stress distribution and elongation are dependent only on total porosity. However, Wagh, (1991) criticized the above expression since it does not involve material's microstructural features like the random shapes of the pores and their random size distribution. Wagh, (1991) developed a model that takes account of the microscopic details of the structure of ceramics (such as alumina, silicon nitride, silicon carbide and $YBa_2Cu_3O_{7-d}$ superconductor), the irregular shapes and size of the pores, and the random distribution of the grain and pore size. The equation developed by Wagh, (1991) is of the form

$$E(p) = E_o(1 - p)^m \quad \dots\dots\dots\dots\dots\dots\dots\dots(2.4)$$

where $E(p)$ is Young's modulus at porosity p, while m is a constant. Some of the relations that have been proposed to relate the elastic moduli of brittle solids to their porosities are given in Table 2.1 below. In Table 2.1, $E(p)$ is the modulus of elasticity at porosity p, E_o is the theoretical elastic modulus at zero porosity, a and n are material constants related to the packing

15

geometry and pore structure of the material, while m, b, h, A and c are simply constants.

TABLE 2.1.

   Some empirical and semi empirical expressions relating porosity to elastic moduli.

Equation	Parameters (E(p))	Source
$E(p) = E_o(1 - p)^m$	Young's	Wagh (1991)
$E(p) = E_o(1 - ap)^n$	Young's	Phani (1986)
$E(p) = E_o\left\{ - (bp + cp^2) \right\}$	Young's	Wang (1984)
$E(p) = E_o(1 - hp)$	Young's	Haynes (1971)
$E(p) = E_o\left[1 - \dfrac{Ap}{1 + (A - 1)p} \right]$	Young's	Hassellman (1964)
$E(p) = E_o \exp(-bp)$	Young's/shear	Knudsen (1959)

As cited in the literature review (section 2.1) such has been done on nondestructive evaluation (NDE) of modern ceramic materials. In Kenya, little or no nondestructive evaluation techniques have been carried out with the aim of characterizing local ceramic products. The present study is therefore aimed at using ultrasonic nondestructive technique to characterize clay based ceramic products fabricated under various conditions.

C H A P T E R   T H R E E

THEORY OF ULTRASONICS

3.0. Introduction

Various kinds of nondestructive evaluation (NDE) technology can be
used to characterize mechanical properties of materials, e.g.,
electromagnetic (eddy currents), radiography and ultrasonics studies,
[Vary *et al*, 1988]. In this study only the ultrasonic technique has
been considered in the characterization of the clay products. The
ultrasonic technique has become one of the generally accepted
techniques for evaluating and comparing product properties, quality
and uniformity of industrial ceramic products [Bhardwaj, 1986]. This
technique allows the detection of areas of low density, and
other defects, hence it permits good overall characterization of
the quality of refractories [Aly, 1985]. It is for this reason that
the technique was chosen for clay material characterization.

The ultrasonic technique depends on measuring physical and acoustical
properties via the interaction of elastic stress waves with
microstructural and morphological features [Fu, 1982].

3.1. Ultrasonic Parameters

The ultrasonic parameters used for material characterization are the
velocity of propagation of the elastic waves, frequency-dependent
attenuation and frequency spectrum changes. Velocity as a parameter is
dependent on the particular combination of material fabricating
conditions and is strongly influenced by the microstructure [Kreher,
1977]. Ultrasonic velocity increases with the decreasing
microstructure dependent porosity. Porosity depends on the shape,

arrangement and the size distribution of the grains. Velocity measurements provide a possible way of determining the mechanical properties of a material [Gaydecki *et al*,1991], for example elastic constants, tensile strength, yield strength [Vary, 1988], residual stress [Vary, 1985], density of sintered ceramics [Klima, 1987; Kupperman *et al*, 1984; Ranachowski, 1975] and porosity [Kreher *et al*, 1977].

Ultrasonic attenuation is related to materials conditions that govern mechanical properties and dynamic response, for example, microstructure [Evans *et al*, 1978; Kreher *et al*, 1977; Mittleman *et al*, 1989] and morphology (grain size, shape, and distribution) [Vary, 1988]. Attenuation measurements can provide information on grain size and shape [Vary,1988], and porosity, [Kunerth *et al*, 1989].

Frequency spectral analysis is based on the principle that the higher frequency components of the propagated pulse are preferentially attenuated with increase in path length than the lower frequencies. Thus the pulse experiences not only a decrease in amplitude with increasing frequency but also a gradual shift of the frequency content to the lower end of the frequency spectrum [Serabian 1968]. Figure 3.1. shows an illustration of a frequency spectrum.

Amplitude
arbitary
units
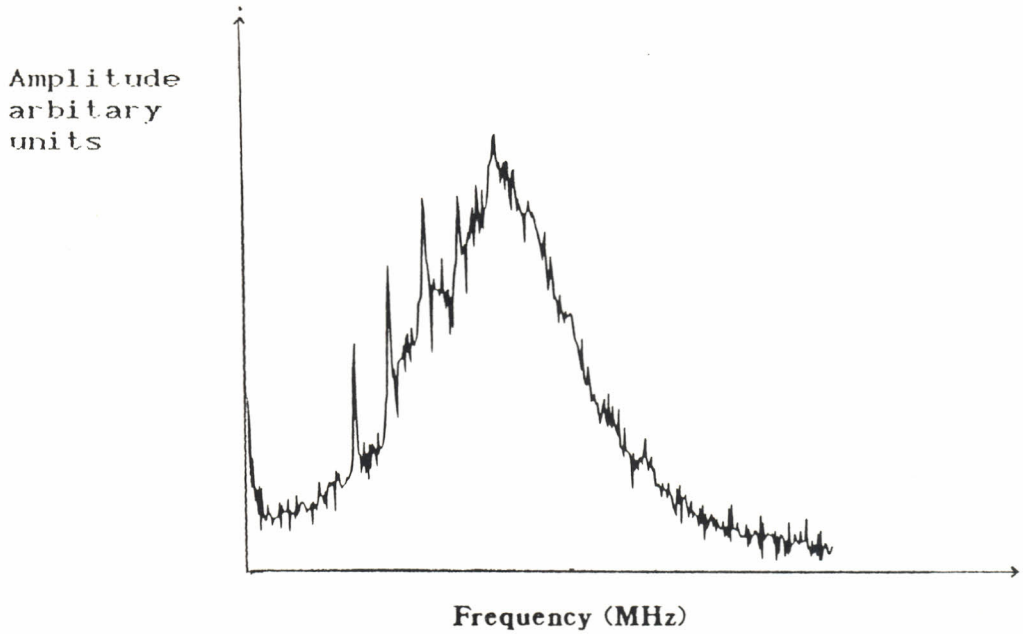
Frequency (MHz)

Fig. 3.1. -An illustration of a frequency spectrum.

3.2. Types of Ultrasonic waves

Depending on the mode of particle vibration relative to the direction
of wave propagation, ultrasonic waves can be classified into three
main categories. When vibrations take place in the direction of wave
motion AB, (Fig. 3.2), longitudinal or compressional waves are said to
be propagated [Blitz, 1964]. The layers in the medium are alternately
compressed and expanded. When vibrations occur in a direction at
right angles to that of the wave motion AB, transverse waves are
propagated (Fig. 3.3). Transverse waves are also known as shear waves
The third category of ultrasonic waves, known as Surface or Rayleigh
waves are characterized by complex motion of longitudinal and

19

shear waves, in which, the vibration direction is perpendicular to the surface of the material AB as shown in Fig. 3.4. [Bhardwaj, 1986]. Surface waves operate within a small `skin´ of the material surface and are attenuated rather rapidly within the bulk. An example of surface waves is the ripples or currents on the surface of water in which rippling is confined only to the surface while underneath the ripples, the material is relatively calm.
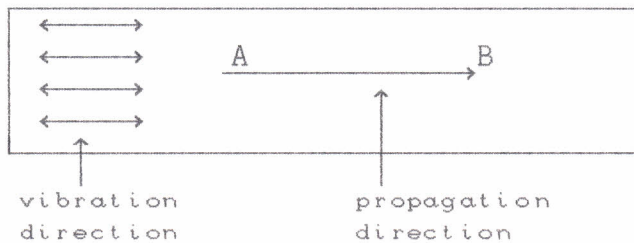
Fig. 3.2. Longitudinal waves
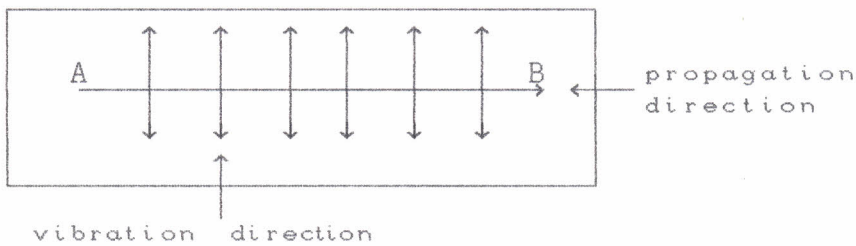
Fig. 3.3. Transverse waves
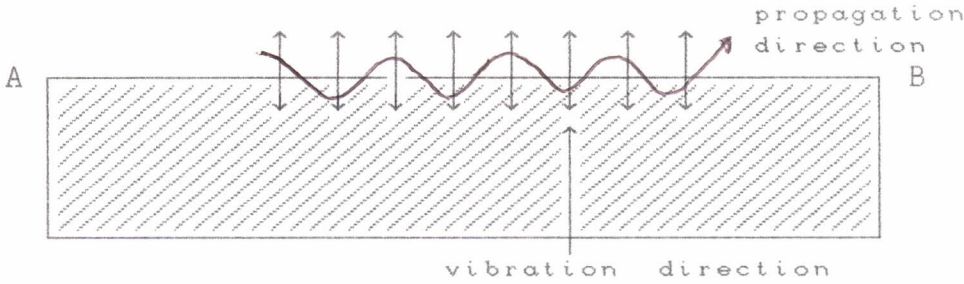
Fig. 3.4. Surface or Rayleigh waves

3.3 Propagation of Ultrasound in Material

When ultrasound is introduced from its source into a material, a variety of phenomena take place. These phenomena are described depending on the direction of wave propagation relative to the material surface [Bhardwaj, 1986].

At the boundary between two different media, the geometry of the propagation of sound is the same as that of electromagnetic waves. Snell's law is valid i.e.

$$\frac{Sin\ \Theta_1}{Sin\ \Theta_2} = \frac{V_1}{V_2} \qquad \dots\dots\dots\dots\dots(3.1a)$$

where V_1 is the velocity of ultrasound in the medium of incidence, V_2 the velocity of ultrasound in the medium of refraction, while Θ_1 and Θ_2 are the angles of incidence and refraction respectively. When ultrasound hits an interface at an oblique angle other than zero, besides transmission and reflection, it is also refracted and its mode

21

converted (e.g. a longitudinal wave may change to a shear wave).
Figure 3.5 shows an example of mode conversion.
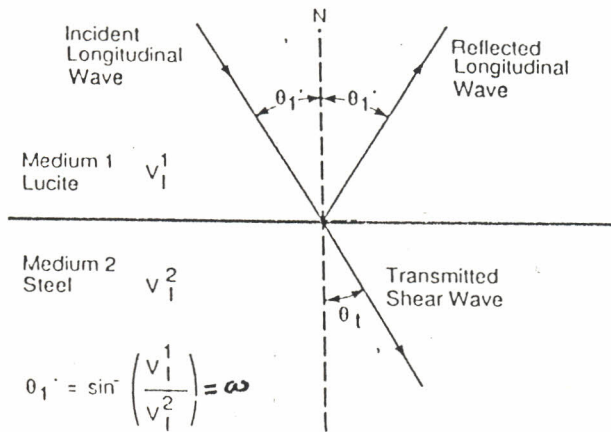
Fig. 3.5. -Generation of shear waves by mode conversion when the incident longitudinal wave is at its first critical angle (ω) or more.

In zero degree of incidence, a part of ultrasonic energy is transmitted into the material while the other is reflected from the material surface (Fig 3.6). The amount of transmission and reflection of ultrasonic energy is defined by the acoustic densities of the medium from which the wave is originating and the medium into which it is propagating [Bhardwaj, 1986]. The alternating

22

displacement of particles in a medium is coupled with alternating pressure called the sound pressure.

MEDIUM 1 | MEDIUM 2

incident wave

$\Longrightarrow$

Transmitted wave

$\Longrightarrow$

Reflected wave

(ρ_1, V_1, Z_1) (ρ_2, V_2, Z_2) $Z_2 > Z_1$

$V_2 > V_1$

$$R = \left(\frac{Z_2 - Z_1}{Z_2 + Z_1} \right)^2 \qquad T = \frac{4 Z_2 Z_1}{(Z_2 + Z_1)^2}$$
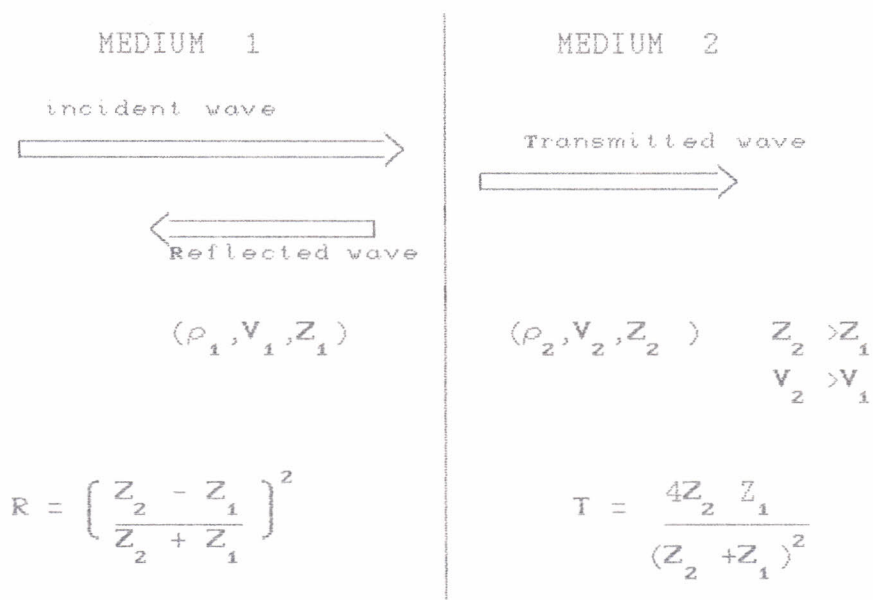
Fig 3.6. Zero degree of incidence of a plane wave from a medium of low acoustic impedance, Z_1, into a medium of high acoustic impedance, Z_2.

The ratio of the sound pressure and particle velocity is the specific acoustic impedance, Z_{sp}, [Drury, 1987]. i.e.

$$Z_{sp} = \frac{\text{sound pressure}}{\text{particle velocity}} \qquad \ldots\ldots\ldots\ldots(3.1)$$

23

and the ratio of the specific impedance Z_{sp} to the cross sectional area (A) across which the sound waves propagate is the acoustic impedance Z_{ac}.

$$Z_{ac} = \frac{Z_{sp}}{A} = R_{ac} + jX \ \ldots\ldots\ldots\ldots(3.2)$$

In Eqn. 3.2, R_{ac} is the acoustic resistance or characteristic impedance and it is associated with dissipation of energy. jX is the reactive term and is due to the inertia and the stiffness of the medium. R_{ac} is given by;

$$R_{ac} = \rho V \ \ldots\ldots\ldots\ldots\ldots\ldots\ldots(3.3)$$

where ρ and V are the density and sound velocity respectively [Frederick, 1965]. Since neglecting the complex term results in no significant difference, then the acoustic impedance is

$$Z_{ac} \cong R_{ac} = \rho V \ \ldots\ldots\ldots\ldots\ldots\ldots(3.3a)$$

If the ratio of the characteristic impedance of the two media is M where

$$M = \rho_2 V_2 / \rho_1 V_1 \ \ldots\ldots\ldots\ldots\ldots\ldots(3.4)$$

then the transmission coefficient (T) and reflection coefficient (R)

will be given   respectively by÷

$$T = \frac{4M}{(M+1)^2} = \frac{4Z_2 Z_1}{(Z_2 + Z_1)^2} \qquad \dots\dots\dots\dots\dots(3.5)$$

$$R = \left[\frac{M-1}{M+1}\right]^2 = \left[\frac{Z_2 - Z_1}{Z_2 + Z_1}\right]^2 \qquad \dots\dots\dots\dots(3.6)$$

and $T + R = 1$ rule is obeyed

3.4. Geometrical Acoustics

Ultrasonic waves from a transducer into a medium of   interest
can be   regarded to have rectilinear propagation. Like all forms of
wave motions, ultrasonic waves also exhibit the   phenomena   of
interference and diffraction. Interference effects are stronger at
some distance close to the transducer. This region is known as   the
near field or Fresnel zone and the extent (near field distance,   NF)
can be calculated from equation 3.7. [Drury, 1987] as

$$NF = D^2/4\lambda \qquad \dots\dots\dots\dots\dots\dots\dots(3.7)$$

In   equation 3.7, D is the   transducer diameter   and λ is   the
wavelength of sound in the material. Due to interference effects,   the
acoustic pressure maxima and minima close to the transducer-face are
rather "crowded" as shown in figure 3.7. If observations are made   in
this region of the wave propagation, slight changes in the   location
of reflectors in the medium would cause significant variations in the

25

amplitude of reflections. Situations may also exist when a reflector may be located on a minimum, yielding no observable reflected signal. Due to these difficulties, observations in the region close to the transducer face [also called "zone of confusion"], are usually avoided. On the other hand, diffraction occurs in the region beyond the first maxima, or the far field also known as Fraunhofer zone. In the Fraunhofer zone, there is no crowding of acoustic pressure maxima and minima.
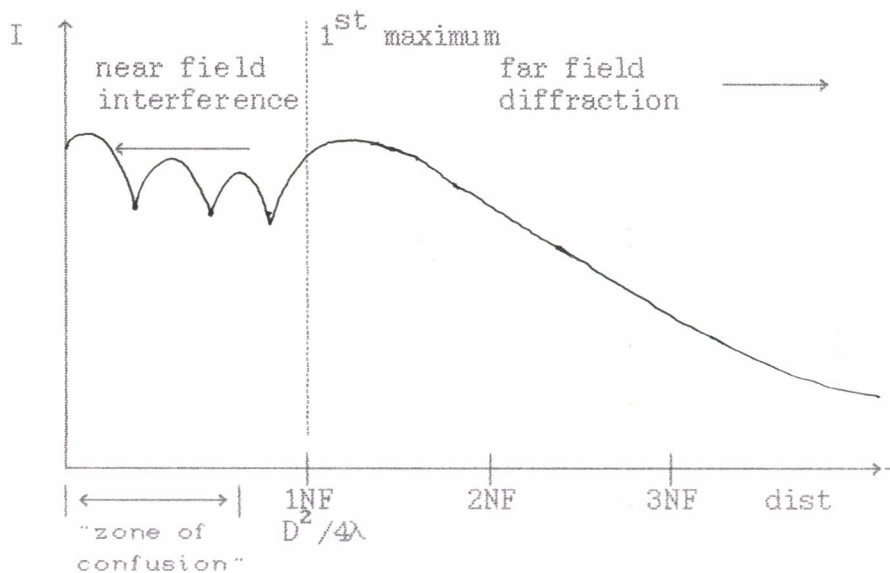
Fig. 3.7. The figure shows the variation of pulse intensity against distance from a probe [After Drury, 1987].

3.5. Ultrasonic Parameters and their Significance

3.5.1. Ultrasonic Velocity

The ultrasonic velocity (longitudinal, transverse or surface) changes in magnitude according to the quality of material (solids, liquids or gases) through which they propagate respectively.

Ultrasonic velocities are related as in equations 3.8 to 3.11, to the properties of the material such as Young's moduli (E), Poisson's ratio (σ) and density (ρ). [Bhardwaj, (1986), Gault, 1989].

$$V_1 = \left\{ \frac{E(1-\sigma)}{\rho(1+\sigma)(1-2\sigma)} \right\}^{1/2} = \left\{ \frac{K + (3/4G)}{\rho} \right\}^{1/2} \quad \ldots\ldots\ldots(3.8)$$

$$V_s = \left[\frac{E}{2\rho(1+\sigma)} \right]^{1/2} = \left\{ \frac{G}{\rho} \right\}^{1/2} \quad \ldots\ldots\ldots(3.9)$$

The shear modulus of elasticity G is given by

$$G = C^2 \rho \quad \ldots\ldots\ldots\ldots(3.10)$$

where C is a constant. And from equations 3.8 and 3.9 we get;

$$E = \frac{\rho V_s^2 \left\{ 3V_1^2 - 4V_s^2 \right\}}{\left\{ V_1^2 - V_s^2 \right\}} \quad \ldots\ldots\ldots(3.11)$$

is defined as a function of frequency. Figure 3.8 shows a general relation of frequency dependence of ultrasonic attenuation.
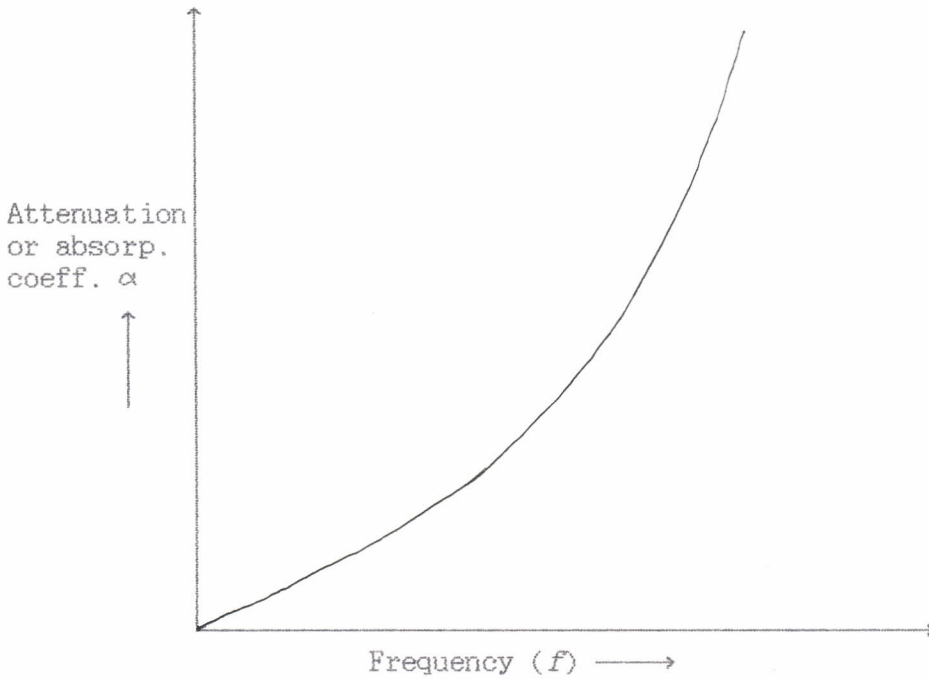
Fig. 3.8 -A schematic relation between frequency and attenuation coefficient, α, frequency dependence of attenuation. (After Bhardwaj, 1986).

The attenuation coefficient can be broken down into two components; the absorption coefficient α_a and the scatter coeffiecient α_s;

$$\alpha = \alpha_s + \alpha_a \qquad \dots\dots\dots\dots\dots\dots(3.13)$$

The absorption is mainly caused by internal friction, elastic hysteresis, heat conduction, dislocation damping and other factors like relaxational phenomena and molecular structure [Vary, 1985; Szilard, 1982]. In solids only the internal friction and elastic hysteresis are dominant. Scattering of ultrasound is caused by any acoustic impedance mismatch occurring in the medium. The scattering regime is closely related to the size of the scatterer with respect to the ultrasonic wavelength in the medium. In polycrystalline aggregates, loss of ultrasonic energy due to scattering, accounts for the greater portion of the losses [Vary, 1985].

Depending on the ratio of the wavelength of the wave to the scatterer diameter, three scattering regions have been identified [Smith *et al*, 1982; Vary, 1985; Gaydecki *et al*, 1991]. If λ is the wavelength, $\mathbb{D}$ the mean diameter of the inhomogeneities, and f the frequency, then for a variety of crystal structures analytic expressions are÷

(a) The Rayleigh scattering range, (i.e. $\lambda \gg \mathbb{D}$.)

$$\alpha_s = C_1 \mathbb{D}^3 f^4 \qquad \dots\dots\dots\dots\dots(3.14)$$

(b) In the Random scattering phase (Stochastic scattering) range, (i.e. $\lambda \cong \mathbb{D}$)

$$\alpha_s = C_2 \mathbb{D} f^2 \qquad \dots\dots\dots\dots\dots(3.15)$$

(c) Diffuse scattering range, $(\lambda \ll \mathbb{D})$,

$$\alpha_s = C_3 / \mathbb{D} \qquad \ldots\ldots\ldots\ldots\ldots\ldots\ldots(3.16)$$

In equations 3.14 to 3.16, α_s is the attenuation due to scattering and C's are single crystal elastic constants. In the Rayleigh scattering region the scatterers can be assumed to be independent. i.e, there is no multiple scattering. This assumption however is not true in the other two regions.

The ultrasonic attenuation can be estimated by comparing the amplitudes of successive reflections from a material. However, this is only true if attenuation does not depend on frequency. On basis of comparison of successive reflections of a pulse, the relative attenuation is estimated using Equation 3.17 [Gieske, 1991].

$$\text{Relative Attenuation (Rel att; } \alpha) = C \log \left\{ \frac{A_{n+1}}{A_n} \right\} \quad \ldots\ldots(3.17)$$

In Equation 3.17, A_{n+1} is the amplitude or voltage of a multiple reflection, A_n is the amplitude or voltage of another reflection immediately preceding A_{n+1}) while C is constant for a given test material.

3.6 Ultrasonic methods.

The methods used in ultrasonic nondestructive evaluation (NDE) technique are classified depending upon the modes of ultrasonic transmission and reception in a test material. In single transducer or

31

the `pulse-echo´ method, a single transducer is used simultaneously as
both the transducer and receiver of ultrasound as shown in figure 3.9.
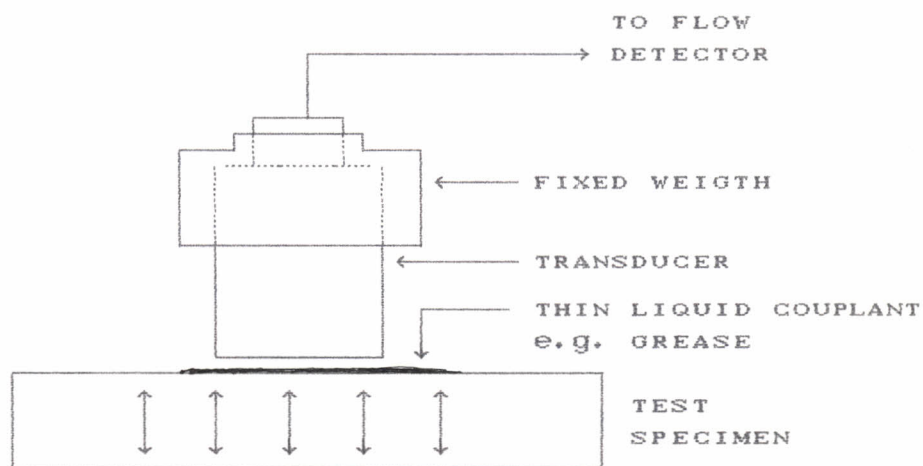
Fig. 3.9 –Single transducer or 'pulse-echo' method
of ultrasonic testing

The transducer can be coupled to the test specimen by direct contact,
solid delay line contact or liquid delay line contact [Bhardwaj, 1986]
In direct contact, the transducer is directly placed or coupled to the
test material surface by a liquid couplant such as oil, grease or
glycerene. The couplant reduces the acoustic impedance mismatch
between the transducer and the test material.

In through transmission method, two transducers are placed opposite
each other on the two surfaces of a test material. One transducer acts
as the transmitter, while the other is the receiver. The other
method used in ultrasonic nondestructive technique is the transmission

32

and reflection or the `pitch-catch´ method. In this method two transducers are placed side-by-side and are slightly angulated and separated by a thin wedge to maximize the ultrasonic response from within the test specimen.

3.7   Attenuation Measurements

The ultrasonic attenuation can be measured by comparing the ultrasonic pulse amplitudes on the cathode ray tube screen of the flaw-detector, either after it has travelled two different known distances in the material in question, or before and after it has travelled a known distance. This is true if there is no dispersion and also if the frequency-attenuation dependence is neglected.

In multiple reflection technique, a fraction of a pulse is picked up by the probe, as the pulse bounces back and forth in the specimen. This provides a measure of the amplitude between each round trip of the pulse.

If the log of the ratio of the two subsequent pulse amplitudes A_{n+1} and A_n (shown in figure 3.10) is denoted by **H** and expressed in decibels as in equation 3.18;

$$ H = -\log \left\{ \frac{A_{n+1}}{A_n} \right\} = \text{Rel. att; } \alpha \quad \ldots\ldots\ldots\ldots(3.18) $$

then, the attenuation coefficient (in decibels per millimeter) for direct contact will be given by equation 3.19 below.

33

CHAPTER FOUR

EXPERIMENTAL DETAILS

4.1a   Materials

Raw clay samples of red firing clay and red hill clay, hereafter designated RFC and RHC respectively were obtained   from   Kenya Industrial Research Development Institute (KIRDI), Nairobi, Kenya.

4.1b. Fabrication of test specimens

The as-received clay samples were further ground   into   fine powder using a pestle and mortar. RFC was ground into finer form than RHC. Particle size distribution of the ground powder was done by wet sieving;   to find the average particle size and to eliminate particles greater than 600 μm.

The clay powders were thereafter moistened with 20% of clean tap water and weighed into small samples of 45.0 ± 0.1 g each from the bulk. The weighed portions were formed at various loading pressures ranging from 64 MPa to 255 MPa into discs of about 5.00 ± 0.01 cm in diameter and about 1.40 ± 0.01 cm in thickness in a hardened   steel   mould (Fig.4.1). Grease was used as a lubricant to prevent sample stickage in the steel mould as well as to reduce friction between the piston and cylinder during compaction. The discs were thereafter left to dry at room temperature ($\cong 22.0^{o}$ C) for about 10 days. The forming of the disc dimensions was chosen following the near field distance (**NF**) value, which by using equation 3.7, was found to be about 1.00 ± 0.01 cm. The values of D and λ used were 10mm and 0.25 cm respectively.

LOAD

LOADING TABLE

STEEL
PISTON

GREASE

CLAY COMPACT

STEEL
SLEEVE

STEEL DISC

FIXED STEEL TABLE
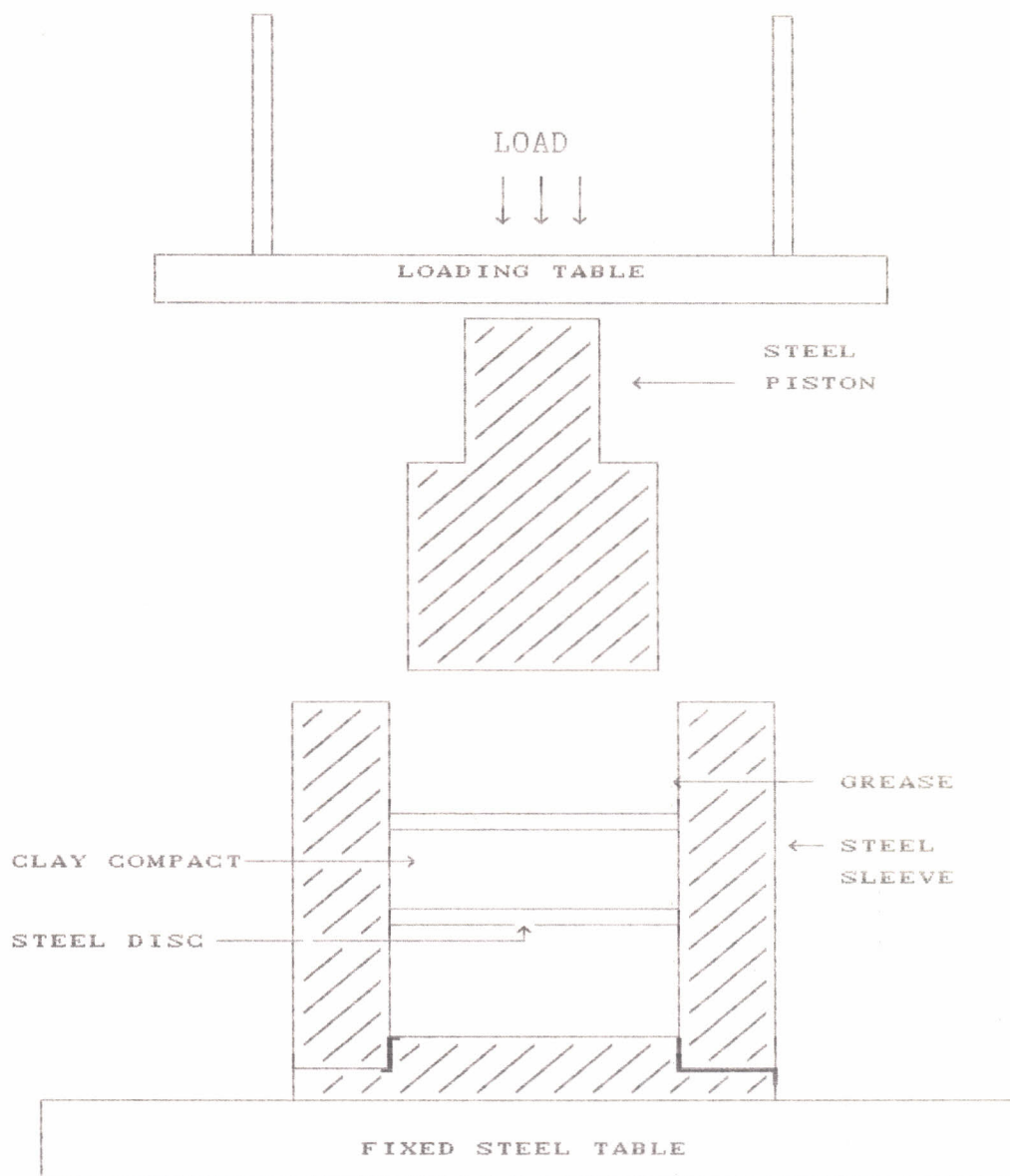
Fig. 4.1. Compacting apparatus

4.2. Firing

Prior to firing, the discs were oven-dried at $\cong 110.0^\circ$ C for two hours to drive off any remaining moisture content. The discs were then fired in an electric furnace to various temperatures as follows; a few discs were heated in the furnace to 200.0° C at the rate of 12.0° C per minute and thereafter soaked at that temperature for two hours. This steady heating rate was necessary on order to prevent exposure of the discs to thermal shock. The furnace temperature was steadily raised at the same rate of 12.0° C per minute to $600.^\circ$C and maintained at that temperature for eight hours. The process was repeated for another lot of discs to $700\ ^\circ$C, $850\ ^\circ$C, and $950\ ^\circ$C respectively.

After firing, the specimens were subjected to natural cooling inside the furnace. This prevented thermal shock, which may cause microcracks in materials [Hefet *et al*, 1992; Orenstein *et al*, 1992].

4.3. Bulk density, porosity and shrinkage measurements

The dimensions and mass of the dried unfired and fired discs were measured for the determination of linear shrinkages and bulk density. The percentage linear drying shrinkage ($\%LDS_f$) on the formed basis and the percentage linear firing shrinkage ($\%LFS_d$) on the dried basis were calculated for each disc using equation 4.1 and 4.2. respectively.

$$\% \ LDS_f = \frac{L_f - L_d}{L_f} \times 100 \quad \ldots\ldots\ldots\ldots(4.1)$$

37

$$\% \ \text{LFS}_d = \frac{L_d - L_F}{L_d} \times 100 \quad \dots\dots\dots\dots(4.2)$$

In the equations 4.1 and 4.2, L_f is the as-formed dimension L_d is the dimension of the dried unfired piece while L_F represents the fired dimension.

The bulk density of each sample was calculated as a ratio of sample mass to its bulk volume. The total porosity P_T in a sample was evaluated using equation 4.3 given below.

$$P_T = 1 - \left[\frac{\rho}{\rho_t}\right] \quad \dots\dots\dots\dots(4.3)$$

In equation 4.3, ρ is the bulk density while ρ_t is the density of a completely dense sample or the true density of a sample. To find the true density of a sample it was necessary to find the true volume V_T of the sample. The true volume of a sample was determined by the water immersion method in which a known weight (30.0 ± 0.1 g) of a sample was immersed in a known volume of boiling water. Boiling water drives off any enclosed air in a sample. The volume of the displaced water was taken to be the true volume (V_T) of a sample. The true density was then evaluated using equation 4.4, given as;

$$\rho_t = \frac{\text{sample dry weight}}{\text{true sample volume } V_T} \quad \dots\dots\dots\dots(4.4)$$

The total porosity of a sample was then evaluated by substituting for ρ_t in equation 4.3 above.

4.4. Mineralogical analysis

Both the X-ray diffraction (XRD) and chemical methods were employed for mineralogical analysis. The XRD patterns for the samples at various firing temperatures were obtained by means of a Philips 1710 diffractometer using Ni filtered CuK_x radiation with a scanning (2θ) of 3-50^0. In chemical analysis samples were first ground to fine powder of 250 mesh. $0.1000 \pm 0.0005g$ mass of a sample was put in a 100 ml plastic container and 0.5 ml of concentrated hydrochloric acid and 0.5 ml of nitric acid added to the mixture in the container. The mixture was left to stand overnight. Thereafter, 3.0 ml of concentrated hydrofluoric acid (HF) was added to the mixture and this again left to soak overnight. 50.0 ml of boric acid was then added and the solution left to stand for an hour. The solution was then topped to 100 ml by adding 46 ml of distilled water. Atomic absorption spectrometry was then carried out on the solutions thereby obtaining the percentage composition of the constituent elements

The mineralogical compositions were calculated by the rational analysis method. Appendix 1 shows the rational analysis method.

4.4. Velocity Measurements

Samples were polished prior to velocity measurements. First, they were polished on wet 600 grit SiC paper and then finished with carborundum 1200 powder. This provided smooth sample surfaces of the order of 1200 mesh. During polishing, care was taken to provide uniform sample thickness.

The longitudinal velocity was obtained by measuring the delay

time of ultrasonic pulses propagated in a clay sample. A single transducer or "pulse and echo" method shown in Figure 3.9 was used. A 2 MHz probe (10 mm in diameter) was employed for measurements. Medium grade petroleum-based grease was used as a couplant. Grease was used since it is a preferable couplant for inhomogeneous surfaces [Gaydecki *et at,* 1992]. Although grease may contaminate porous samples, no possible contamination was observed with the samples used in this study. A small weight was attached to the transducer to ensure a constant coupling force at the sample-to-probe interface. Measurements were made at three locations on each test disc, averaged and recorded.

The measured ultrasonic longitudinal velocity (V_1) was evaluated from equation 4.5.,

$$V_1 = 2d/t \qquad \dots\dots\dots\dots\dots\dots\dots\dots\dots\dots\dots\dots(4.5)$$

where d is the thickness of the test piece and t represents the time taken for a sound wave to make a round trip through the thickness.

4.5. Ultrasonic attenuation measurements

The ultrasonic attenuation was determined by comparing the ratio of two subsequent amplitudes A_{n+1} and A_n as seen previously in figure 3.8. However, the following assumptions were made [Bilgutay *et al*,1988]:

(a) The energy due to multiple scattering was assumed negligible (i.e. Rayleigh scattering was assumed since the ultrasonic wavelength was generally much larger than the

C H A P T E R   F I V E

EXPERIMENTAL   RESULTS   AND   DISCUSSIONS

The results obtained are given and discussed below:

5.0   Characteristics of fired clays

5.1   Particle size distribution

Tables 5.1a and fig. 5.1 show the particle size distribution in the
clay samples. RFC samples were found to have a higher percentage of
`finer´ particles than RHC samples as shown in Table 5.1b. The
particle sizes less than 75 μm in RFC and RHC were 96.7% and 87.8%
respectively. This difference in the particle size distribution
observed in the RFC and RHC was due to the grinding of the as-received
clays. RFC samples were ground into more finer form than RHC samples.

5.2.   Chemical composition

The chemical analysis of the raw and fired samples are presented in
Table 5.2a. Compositionally, both the raw clay samples were rich in
silica and alumina with raw RHC having the highest percentage of
silica (76.7%) and a lower amount of alumina (21.5%). Raw RFC had
65.4% of silica but a slightly   higher amount of alumina (22.3%)
compared to the 21.5% in RHC.

In fired RHC samples, an overall decrease in the composition of SiO_2
was observed with increasing firing temperature. In fired RFC samples,
an increase in SiO_2 content was noted with increasing   firing
temperature. The composition of Al_2O_3 in both RFC and RHC generally
decreased with increase in firing temperature. Also in Table 5.2a, it

was noted that the composition of fluxes (i.e. TiO_2, Fe_2O_3, CaO, Na_2O, K_2O, and MgO) in both RFC and RHC samples increased as the firing temperature was increased. Further, RHC samples had higher percentage of fluxes compared to RFC samples for any particular firing temperature.

T A B L E 5.1a

Particle size distribution of the clays

Particle size (x)	Total percentage	
	RHC	RFC
425μm <x< 600μm	6.0	0.9
300μm <x< 425μm	2.2	0.3
212μm <x< 300μm	2.0	0.4
150μm <x< 212μm	2.0	1.7
75μm <x< 150μm	3.2	10.6
x< 75μm	84.6	86.1

The clay samples were classified according to particle sizes as follows; silt (x<75 μm), fine sand (75 <x<212 μm), and medium sand (212<x<600 μm). Based on this classification, the percentage compositions in the clay samples is shown in Table 5.1b.

43
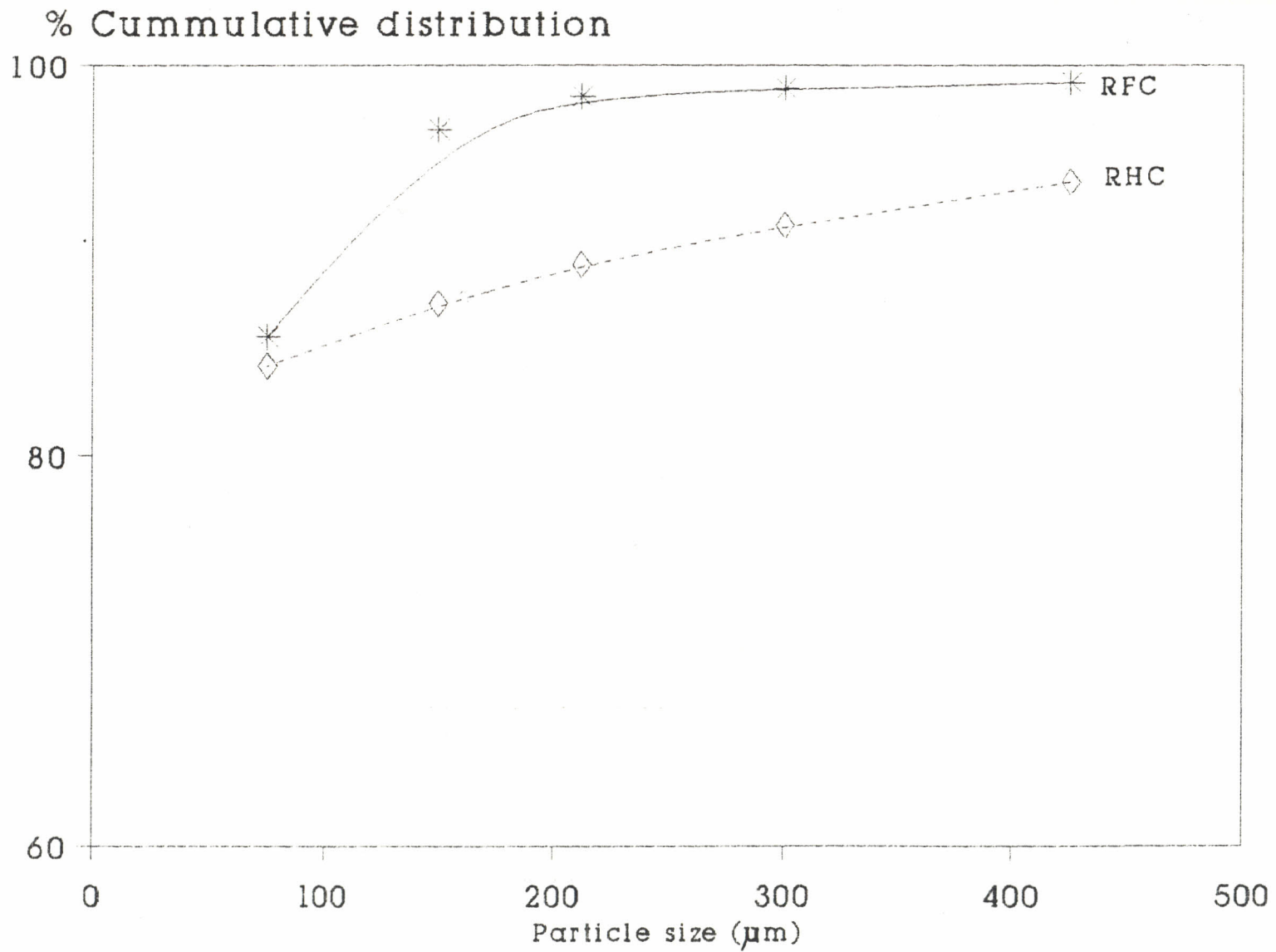
FIG. 5.1

Fig. 5.1 Particle size distribution of the clay samples

TABLE 5.1b

Percentage classification of clay particle sizes.

% composition of	Clay sample	
	RHC	RFC
silt	84.6%	86.1%
fine sand	5.2%	12.3%
medium sand	10.2%	1.6%

The Al_2O_3 is a major constituent of the clay mineral-Kaolinite ($AL_2O_3.2SiO_2.2H_2O$). This clay mineral decomposes at temperatures as low as 450 ^{O}C into metakaolinite ($Al_2Si_2O_7$). Such a reaction was probably the major cause for the observed general decrease in the composition of Al_2O_3 as the temperature was increased. On the other hand, SiO_2 exists as free quartz as well as a constituent in other clay minerals such as kaolinite, Soda mica ($Na_2O.$ $3Al_2O_3.6SiO_2.2H_2O$) and Potash mica ($K_2O.3Al_2O_3.6SiO_2.2H_2O$). These minerals decompose or transform with temperature. These transformations subsequently alter the compositions of the respective constituent oxides such as Al_2O_3 and SiO_2. For example micas have dehydration characteristics remarkably similar to those of kaolinite [Worrall, 1986]. Further, Quartz (SiO_2) is coarse grained and reacts with other fluxes although a little. The observed high composition of fluxes in RHC samples is probably due to the source of this type of clay. As earlier stated in introductory chapter, RHC was obtained from volcano ashes. Volcano clays have high proportions of fluxing ions comparable to clays found in plateaus [worrall, 1986].

45

T A B L E 5.2a

chemical analysis of clay samples

| ELEMENT OXIDES | RAW AND FIRED CLAY SAMPLES (wt%) | | | | | | | |
| | RFC | | | | RHC | | | |
	raw	600c	700c	950c	raw	600c	700c	950c
SiO_2	65.4	72.8	73.6	68.8	76.7	71.6	70.3	73.6
TiO_2	1.2	1.4	1.4	1.1	1.3	1.2	1.2	1.2
Fe_2O_3	4.8	4.6	4.9	6.9	4.7	7.3	7.1	7.6
CaO	0.3	0.4	0.4	0.7	0.4	0.6	0.7	0.7
Na_2O	0.5	0.6	0.6	2.7	0.5	2.7	2.6	2.9
K_2O	0.7	0.8	0.8	2.7	0.8	2.9	2.8	2.9
Al_2O	22.3	21.1	19.7	17.6	21.5	18.2	19.8	18.1
MgO	0.2	0.2	0.2	0.3	0.3	0.3	0.3	0.3
Fluxes	7.7	8.0	8.3	14.4	8.0	15.0	15.1	15.2

5.3. Mineralogy

The results obtained by rational analysis for the composition of
minerals present in the clay samples is given in Table 5.2b. The X-ray
patterns are shown in Fig 5.2. From both Table 5.2b and figure 5.2, it
was observed that the major minerals in raw samples were kaolinite and
quartz and low amounts of micas. From rational analysis, it was found

that raw RHC contained higher amount of quartz i.e, 51.4 % while in RFC, kaolinite was the major mineral, constituting 45.1 %.

T A B L E 5.2b

Rational analysis of clay samples

CLAY MINERALS	RAW AND FIRED CLAY SAMPLES (wt%)							
	RFC				RHC			
	raw	600c	700c	950c	raw	600c	700c	950c
Soda mica	6.17	7.03	6.91	32.9	6.66	33.3	32.4	35.4
Potash mica	5.92	6.43	6.97	6.77	6.68	24.2	24.0	24.6
Kaolinite	45.1	40.1	36.3	4.65	41.2	4.41	6.56	5.11
Quartz	39.1	18.3	30.4	48.1	51.4	42.9	39.1	43.4
Miscellaneous oxides, organic matter etc.	3.68	28.2	19.4	5.59	–	–	–	–

In fired samples, X-ray patterns showed higher peaks for mica and feldspar while the peak intensities of kaolinite dropped especially in RFC (see Table 5.2). Rational analysis indicated a drastic increase in the percentage of mica and a drop in the percentage of kaolinite at

47

RAW RFC

RFC AT 700°C

RFC AT 950°C

Q – Quartz

M – Mica

K – Kaolinite

F – Feldsper

RAW RHC

RHC AT 700°C

RHC AT 950°C

35°   30°   25°   20°   17°

2θ
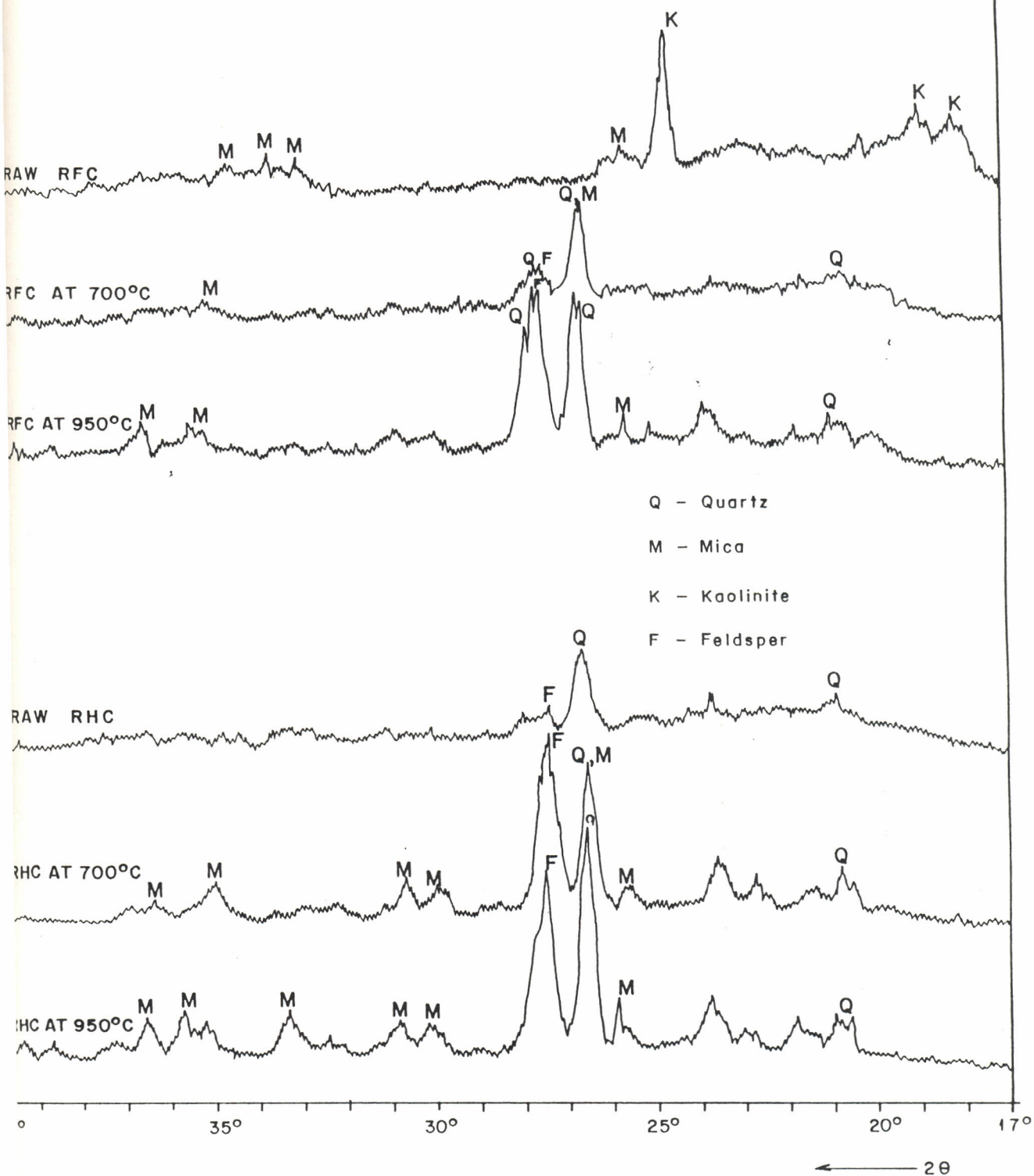
Fig. 5.2 – X ray patterns of clay samples .

48

temperatures where the respective chemical constituents of these minerals increased and dropped respectively.

The decrease in kaolinite content was probably due to its decomposition by losing its hydroxyl groups as water according to reaction below; [Worrall, 1986; Nosbusch et al, 1986].

$$Al_2Si_2O_5(OH)_4 \xrightarrow{\ 450\,^{O}c\ } Al_2Si_2O_7 + 2H_2O$$

$$\text{Kaolinite} \qquad\qquad\qquad\qquad \text{Metakaolin}$$

However this dehydration may occur at $600\,^{O}c$ for well-crystallised kaolinite and at about $580\,^{O}c$ for all kaolinite, [Worrall, 1986].

5.4 Drying and firing shrinkage

The results calculated as a percentage of the dry size i.e. the percentage linear drying shrinkage (% LDS_f) and the percentage linear firing shrinkage (%LFS_d) at various processing conditions are given in Tables 5.3 and 5.4, and plotted in figures 5.3 and 5.4 respectively.

From Fig. 5.3, the linear drying shrinkage in both RFC and RHC samples was observed to fall almost linearly with increasing compaction pressure. RFC samples were observed to have higher percentage of drying shrinkage compared to RHC samples.

The percentage linear firing shrinkage (%LFS_d) in the clay samples was observed to increase with increasing firing temperature as shown in

49

Fig. 5.4. RFC samples were again observed to have higher percentage of firing shrinkage compared to RHC samples. Again the trend of variation was nearly linear. Such a linear variation of firing shrinkage with temperature has been observed in some Nigerian clays [Ibisi, 1991].

Kshama *et al*, (1992) has observed that high values of wet to dry shrinkage are usually associated with a high proportion of fine particles. Further, larger particle size clays have poor plasticity and strength and show faster dewatering, lower drying and firing shrinkage. As seen from Table 5.1a and Fig. 5.1, RFC had a higher percentage of `finer´ particles and hence would be expected to have higher shrinkage values, both drying and firing shrinkage. This is in line to our findings that samples of RFC had higher firing shrinkages than those of RHC.

T A B L E 5.3

The linear drying shrinkage of the clay samples

Compaction Pressure (± 2.5MPa)	Percentage LDS_f	
	RFC Samples	RHC Samples
64.0	9.00	3.40
	9.00	3.80
	7.60	3.40
	7.40	3.20
	8.40	3.20
	8.00	3.00
	8.00	3.40
128.0	7.20	3.00
	7.40	3.20
	7.00	3.20
	8.00	3.00
	7.60	3.20
	7.60	3.40
	7.40	3.40
	7.40	3.00
	7.20	3.20
	7.20	3.20
255.0	7.60	2.00
	7.40	2.60
	8.00	2.40
	7.20	2.60
	7.40	2.60
	7.00	2.40
	6.80	2.00

FIG. 5.3
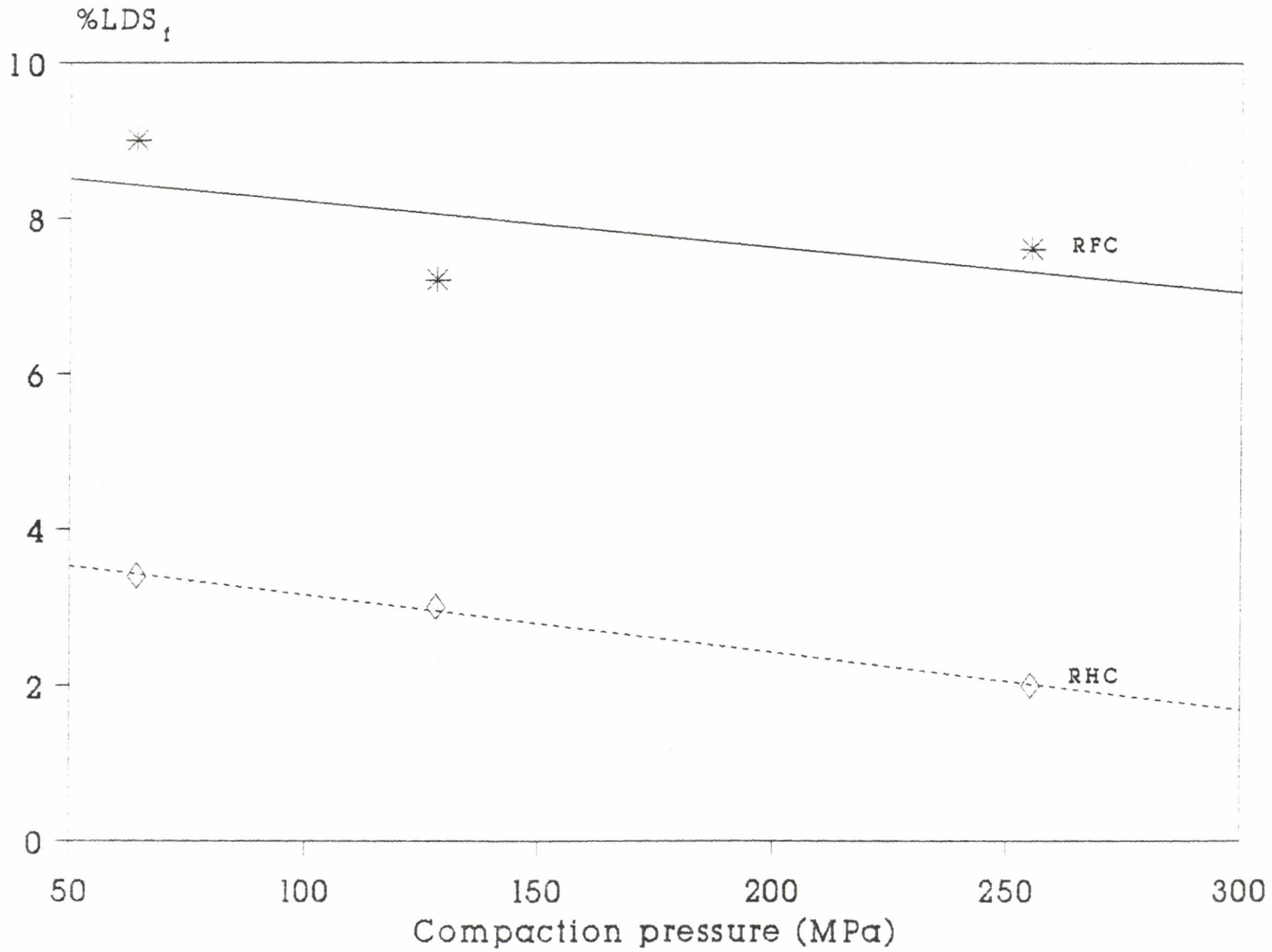
Fig. 5.3 Variation of the %LDS with compaction pressure

T A B L E 5.4.

The linear firing shrinkage of the clay samples

Compaction Pressure (±2.5MPa)	Firing Femp. (±10°c)	Average percentage LFS$_d$	
		RFC	RHC
64.0	600.0	1.970	0.640
	700.0	2.309	0.900
	850.0	2.510	1.100
	950.0	2.647	1.250
128.0	600.0	0.867	0.520
	700.0	1.295	0.750
	850.0	1.835	0.870
	950.0	1.945	0.970
255.0	600.0	0.800	0.450
	700.0	1.180	0.730
	850.0	1.500	0.810
	950.0	1.700	0.880

FIG. 5.4

%LFS$_d$

RFC

RHC

Firing temperature (θ c)
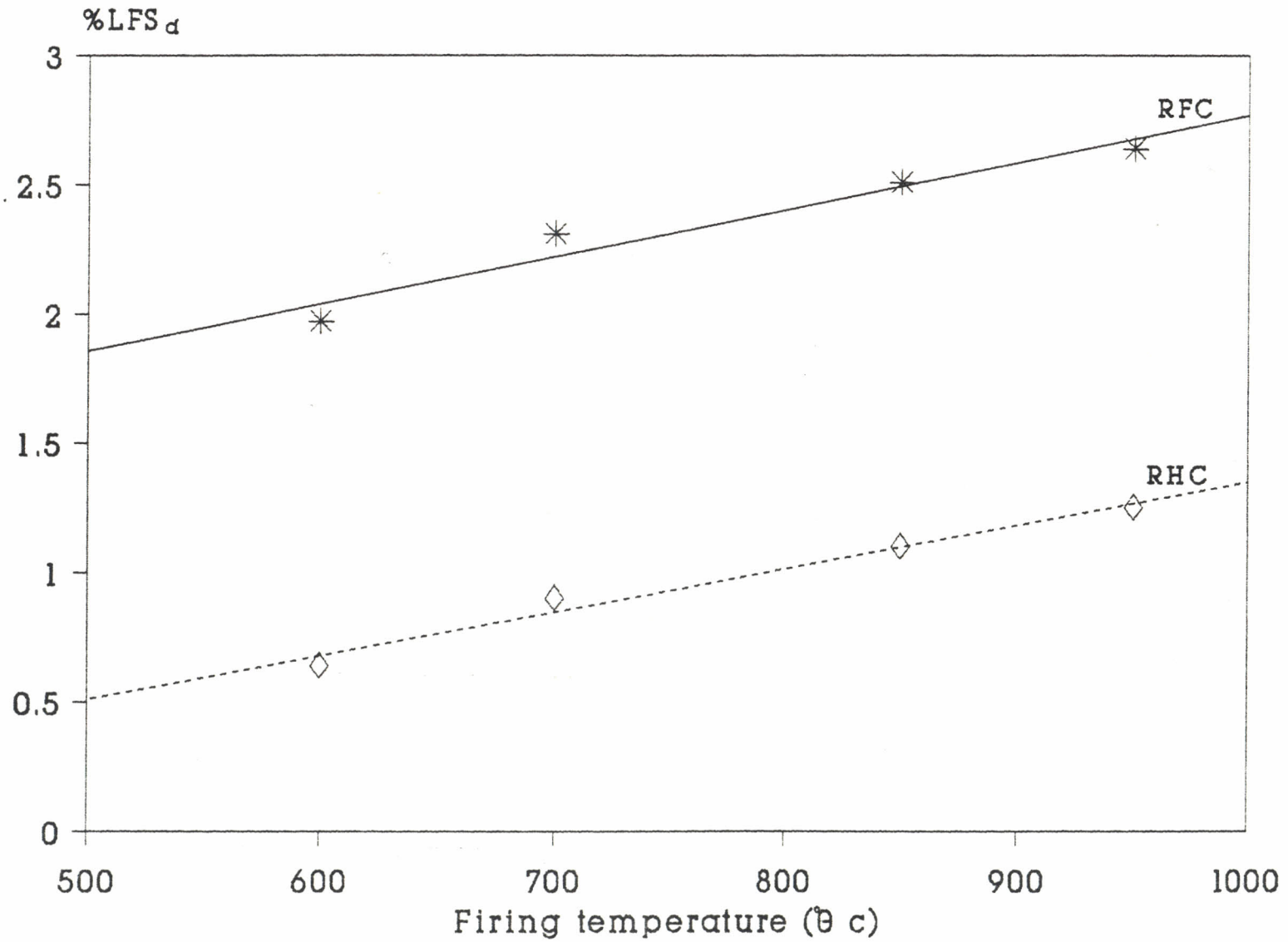
Fig. 5.4 Variation of the %LFS$_d$ with firing temperature

5.5. Bulk density and porosity

The bulk density (ρ) values for the samples fabricated at various processing conditions are given in Table 5.5. The average true densities (ρ_t) in RFC and RHC were found to be 2.140 ± 0.001 g/cm^3 and 2.220 ± 0.001 g/cm^3 respectively.

Figure 5.5 shows the variations of bulk density with compaction pressure at various firing temperatures (following Table 5.5). In all cases, bulk density increased with increasing compaction pressure and firing temperature. Kobayashi et al, (1992) have reported a similar trend in porcelain bodies. Kobayashi *et al*, (1992), observed an increase in density with firing temperature upto a maximum followed by a drop with further increase in firing temperature as was shown in Fig 2.5. However, such observations were not possible in our study since our samples were fired upto only a maximum of 950°C.

The effect of compaction pressure on bulk density shown in Fig 5.5, was more pronounced in RFC samples than in RHC samples. The former showed the highest increment rates in bulk density as the compaction pressure was increased. Below the compaction pressure of 190 MPa, RHC samples had higher density values compared to RHC samples fired at the same temperature. This was because, from chemical analysis (Table 5.2a) RHC samples contained a high percentage of fluxes (Fe$_2$O$_3$, Na$_2$O, K$_2$O, CaO and MgO) which constituted denser elements. However, above compaction pressures of 190 MPa the bulk density of RFC samples were higher than those of RHC samples due to the high densification rate in RFC samples attributed to its high percentage of finer particle size distribution. Since

T A B L E 5.5

Sample bulk densities at various processing conditions

Firing Temperature ($\pm 10^{o}$c)	Compaction Pressure (± 2.5MPa)	Disc bulk densities (ρ) g/cm^3	
		R.F.C.	R.H.C.
600.0	64.0	1.536	1.592
		1.545	1.596
		1.545	1.593
	128.0	1.549	1.613
		1.584	1.608
		1.557	1.612
		1.610	1.612
	190.0	1.624	1.625
		1.636	1.635
		1.641	1.630
	255.0	1.642	1.630
		1.660	1.628
		1.652	1.632
700.0	64.0	1.548	1.613
		1.543	1.610
		1.543	1.612
	128.0	1.592	1.631
		1.612	1.629
		1.612	1.629
	190.0	1.648	1.645
		1.651	1.651
		1.653	1.643
	255.0	1.680	1.662
		1.668	1.655
		1.668	1.650

T A B L E 5.5 cont.

Sample bulk densities at various processing conditions

Firing Temperature ($\pm 10^{\circ}$c)	Compaction Pressure (± 2.5MPa)	Disc bulk densities (ρ) g/cm^3	
		R.F.C.	R.H.C.
850.0	64.0	1.548	1.630
		1.545	1.628
	128.0	1.607	1.642
		1.620	1.643
		1.618	1.643
	190.0	1.667	1.655
		1.660	1.653
		1.663	1.653
	255.0	1.679	1.665
		1.685	1.663
		1.683	1.663
950.0	64.0	1.550	1.635
		1.552	1.629
		1.549	1.637
	128.0	1.622	1.646
		1.631	1.651
		1.628	1.648
	190.0	1.668	1.665
		1.666	1.663
		1.671	1.660
	255.0	1.692	1.670
		1.689	1.671
		1.685	1.673

FIG. 5.5

Disk bulk density (g/cm^3)
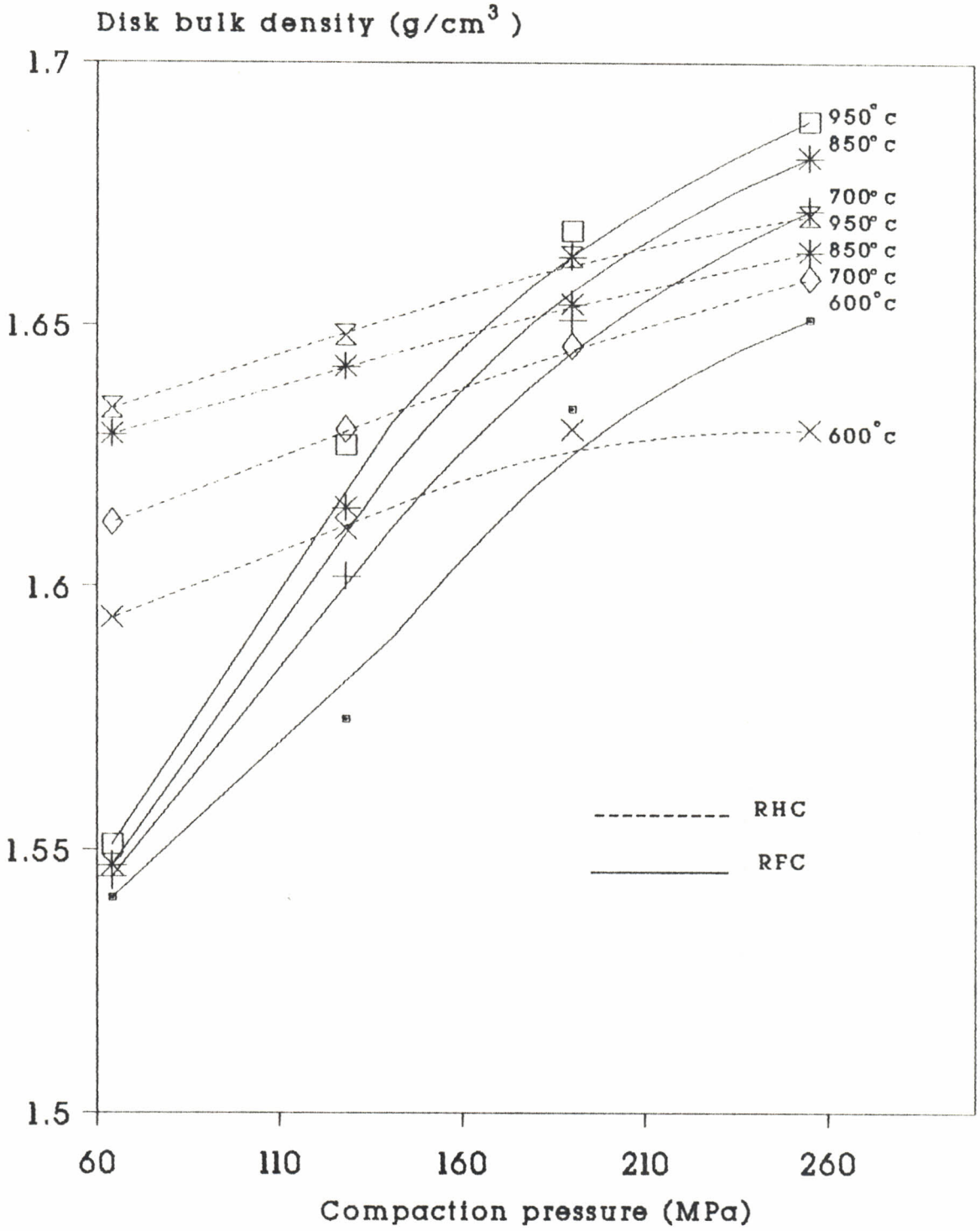
Fig.5.5 Bulk density variation with compaction pressure

sample densification is dependent on the initial fabrication conditions such as the shape, size, size distribution and mode of packing of particles, a sample with a `finer` particle size distribution will be expected to be denser than a sample with `coarser` particle size distribution when the two are compacted at the same conditions. At high compaction loads (> 230 MPa) one expects a lower rate of densification in both the two types of clay samples. This is because the grains flatten out becoming oval in shape; [Kendall, 1990; Knudsen, 1959].

It was also observed that the densification rate in both clay samples slowed down at temperatures above 750°C. This trend of variation in bulk density with firing temperature could be attributed to the processes that occur during firing, such as a decrease in the specimens total surface area. In the process of firing, a decrease in the specimen's total surface area (dependent on the shape, size, size distribution and modes of packing of the particles) occurs [Nosbusch *et al* 1986].

In the initial firing stages the predominant feature is an increase in the inter-particle contact areas with time accompanied by a rounding off of the sharp re-entrant angles at the points of contact. These can lead to the development of microstructural imperfections that may dominate the performance of the fired ceramic ware [Waiser et al 1986]. Also still in this early stages of firing, water vapour is formed and exerts pressure on the solid matrix, giving rise to microcracking or re-opening of pre-existing cracks or microcracks [Arnould *et al* 1985]. During these

59

geometrical changes and subsequent specimen densification, the distances between particle centers decreases. (Stewart, 1962). This decrease in the distance between particle centers results in a decrease in the volume of the inter-particle pore spaces which at this stage are interconnected. In this stage, the densification rate is higher as was observed in Fig. 5.4. At high temperatures of about 800° C, slower densification resulting from low rate shrinkage is observed and this is expected to go on until the minimum number of closed and isolated pores are attained.

In this study, the highest bulk density was 1.685 ± 0.001 g/cm^{3} at 255 MPa, 950°C and the lowest bulk density was 1.536 ± 0.001 g/cm^{3} at 64 MPa, 600°C. Both these values were reported in RFC samples. RHC samples had medium bulk density values with a maximum of 1.673 ± 0.001 g/cm^{3} at 255 MPa, 950°C and a minimum of 1.592 ± 0.001 g/cm^{3} at 64 MPa, 600°C. The behaviour of the apparent porosities were the reverse of the corresponding densities as was expected.

5.6. Ultrasonic velocity

The results relating to longitudinal velocity in the samples are described as follows:

The longitudinal velocities (V_l) obtained at various sample bulk densities (porosities) are given in Tables 5.6 and 5.7 for RFC and RHC samples respectively.

Figure 5.6 shows a linear variation of the measured ultrasonic velocity with bulk density. while in Fig. 5.7, the variation of the longitudinal velocity with porosity is shown. In these figures, it was observed that in both RFC and RHC samples, the longitudinal velocity increased with increasing sample bulk density (Fig. 5.6) or decreasing sample porosity (Fig 5.7). This observation was within the porosity range of investigation i.e. 20.9 % to 28.2 %. Further, the measured velocity values in RFC samples were observed to be higher than those in RHC samples at same porosities.

These observations are is in agreement with results that velocity decreases as porosity increases [Gaydecki et al, 1992; Ranachowski, 1975]. Despite the fact that below a compaction pressure of 190 MPa RHC samples were denser than RFC samples (Fig 5.6), velocity values in RFC samples were consistently higher than those in RHC samples. This showed that ultrasonic velocity was affected by the microstructure (propably pore sizes). The coarser particle size distribution in RHC samples compared to that in RFC samples may have resulted in larger pores which consequently reduced the speed of sound waves in these products.

61

T A B L E 5.6

Measured longitudinal velocities in RFC samples at various
sample densities and porosities

Firing Temprature ($\pm 10^{o}$C)	Compaction Pressure (± 2.5MPa)	Bulk Densities (ρ) g/cm^3	Sample Porosity (p)	Ultrasonic Velocity. (V) m/s
600.0	64.0	1.536	0.282	4121.7
		1.545	0.278	4075.5
	128.0	1.549	0.276	4216.1
		1.584	0.260	4300.1
		1.557	0.272	4244.7
		1.610	0.250	4502.2
	190.0	1.624	0.241	4858.5
		1.636	0.236	5020.1
		1.641	0.233	5145.3
	255.0	1.642	0.233	5110.4
		1.660	0.244	5150.5
		1.652	0.228	5250.3
700.0	64.0	1.548	0.276	4140.9
		1.543	0.279	4102.9
	128.0	1.592	0.256	4585.4
		1.592	0.256	4482.3
		1.612	0.247	4641.2
	190.0	1.648	0.230	4923.0
		1.651	0.229	5240.7
		1.653	0.228	5262.1
	255.0	1.680	0.215	5267.4
		1.680	0.215	5298.4
		1.668	0.221	5287.3

T A B L E 5.6 cont.

Measured longitudal velocities in RFC samples at various sampl
densities and porosities

Firing Temprature ($\pm 10^{\circ}$C)	Compaction Pressure (± 2.5MPa)	Bulk Densities (ρ) g/cm^3	Sample Porosity (p)	Ultrasonic Velocity. (V) m/s
850.0	64.0	1.548	0.276	4281.1
		1.545	0.278	4257.9
	128.0	1.607	0.250	4810.6
		1.620	0.243	5062.1
		1.618	0.244	5060.7
	190.0	1.663	0.223	5592.9
		1.660	0.224	5645.3
		1.667	0.221	5517.9
	255.0	1.679	0.215	5420.0
		1.685	0.213	5580.3
		1.683	0.214	5520.9
950.0	64.0	1.550	0.276	4262.7
		1.552	0.275	4325.3
		1.549	0.276	4266.7
	128.0	1.622	0.242	5207.3
		1.631	0.236	5295.1
		1.628	0.239	5257.3
	190.0	1.666	0.221	5558.6
		1.668	0.221	5593.6
		1.671	0.219	5597.6
	255.0	1.692	0.209	5701.0
		1.689	0.211	5755.0
		1.685	0.213	5634.6

T A B L E 5.7

Measured longitudinal velocities in RHC samples at various sample densities and porosities

Firing Temprature $(\pm 10^o C)$	Compaction Pressure $(\pm 2.5 MPa)$	Bulk Densities (ρ) g/cm^3	Sample Porosity (p)	Ultrasonic Velocity. (V) m/s
600.0	64.0	1.593	0.282	3775.0
		1.592	0.282	3640.3
		1.596	0.281	3700.3
	128.0	1.612	0.274	3820.1
		1.613	0.274	3816.1
		1.608	0.277	3809.8
	190.0	1.625	0.268	3902.0
		1.635	0.264	3962.0
		1.630	0.266	3920.5
	255.0	1.630	0.266	3930.4
		1.628	0.267	3945.0
		1.632	0.265	3862.1
700.0	64.0	1.612	0.274	3810.1
		1.613	0.274	3862.2
		1.610	0.275	3841.3
	128.0	1.631	0.265	4060.1
		1.629	0.267	4059.5
		1.629	0.267	3985.7
	190.0	1.645	0.260	4102.0
		1.643	0.259	4125.4
		1.651	0.256	4141.8
	255.0	1.655	0.256	4100.0
		1.662	0.251	4221.1
		1.650	0.256	4141.0

easured longitudinal velocities in RHC samples at various

ensities and porosities

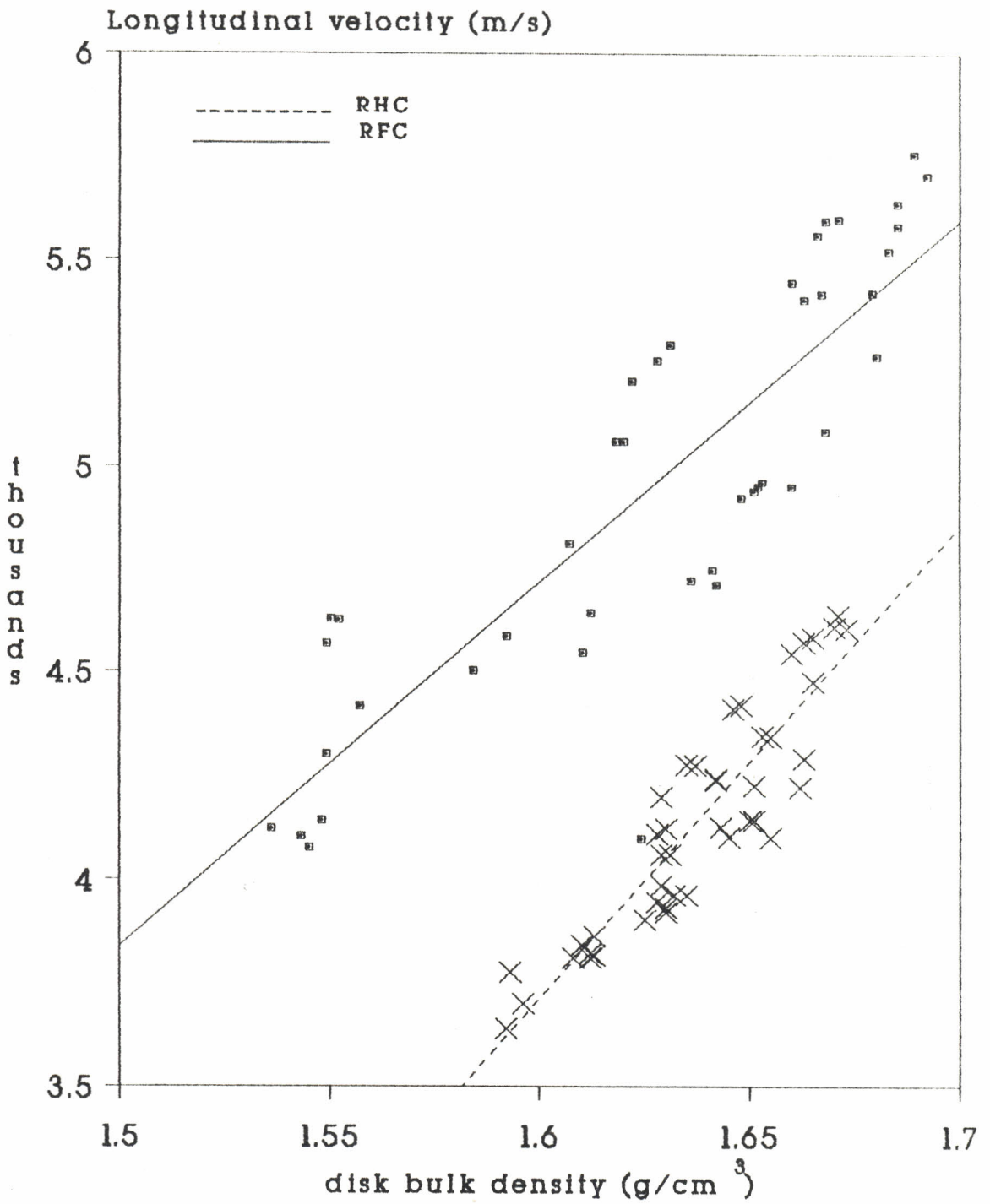| Firing Temprature ($\pm 10^{o}C$)	Compaction Pressure ($\pm 2.5MPa$)	Bulk Densities (ρ) g/cm^3	Sample Porosity (p)	Ultrasonic Velocity. (V) m/s
850.	64.0	1.630	0.266	4121.1
		1.628	0.267	4107.8
		1.630	0.266	4121.1
	128.0	1.642	0.259	4240.0
		1.642	0.259	4236.7
	190.0	1.655	0.256	4342.1
		1.653	0.256	4344.1
	255.0	1.665	0.251	4474.1
		1.663	0.251	4289.4
950.0	64.0	1.635	0.264	4275.0
		1.637	0.263	4004.1
		1.629	0.267	4197.8
	128.0	1.646	0.260	4210.1
		1.648	0.258	4318.2
		1.651	0.256	4225.0
	190.0	1.665	0.250	4461.0
		1.660	0.252	4443.8
		1.663	0.251	4369.9
	255.0	1.670	0.248	4500.0
		1.673	0.246	4093.8
		1.671	0.247	4435.42

FIG. 5.6

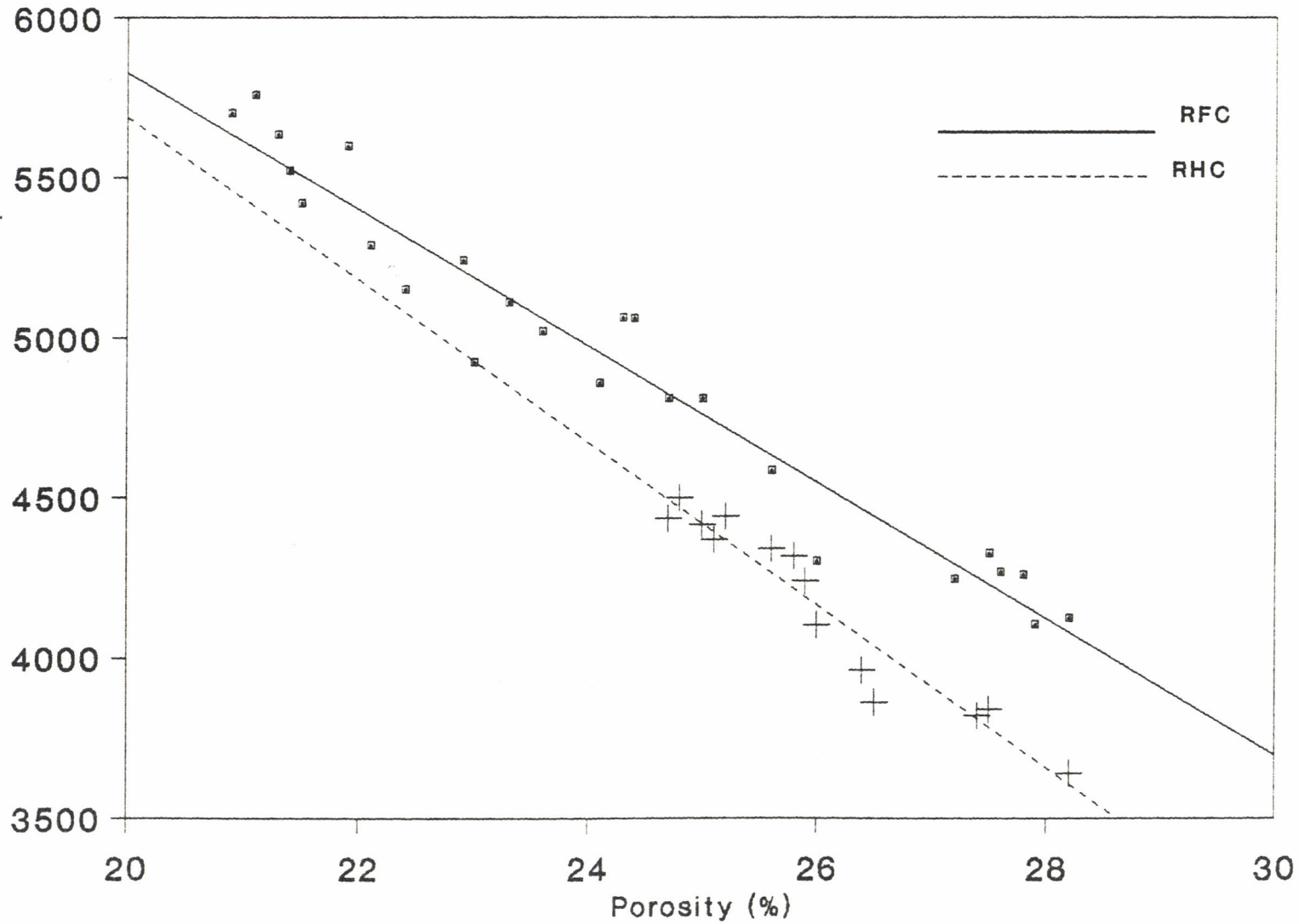Fig.5.6 Variation of long. velovity with bulk density

Fig. 5.7 -Plot of longitudinal velocity versus porosity

Fig 5.8 shows the variation of the average longitudinal velocities in the samples with sample firing temperature for various loading pressures. From figure 5.8, it was observed that the speed of sound increased with sample firing temperature with most samples showing a higher rate of increase in longitudinal velocity at temperatures upto $750^{O}C$. The rate of increase of sound velocity with temperature slowed down in most samples at temperatures above $750^{O}C$. Gieske *et al*,(1991) have also reported an increase in ultrasonic longitudinal velocity with firing temperature upto $1200^{O}C$ in fused silica. In our study it was further noted that for samples of both clays compacted at 255 MPa and at 190 MPa, the measured velocities were not much different. This is in contrast to the cases when the compaction pressures were between 64 MPa and 128 MPa.

From previous results; (Fig 5.5) it was noted that the bulk density had a higher rate of increase between temperatures of $600^{O}C$ and $750^{O}C$ and loading pressure of 64 MPa and 190 MPa. A similar trend in the longitudinal velocity within this same range of temperature and compaction pressure was expected since the dependence of longitudinal velocity on sample bulk density was linear. The linear dependence means that the variation of longitudinal velocity with compaction pressure and firing temperature should be similar to the variation of bulk density with compaction pressure and firing temperaturew respectively. This shows that the wave speed is dependent on initial sample processing conditions, in this case the firing temperature and compaction pressure.
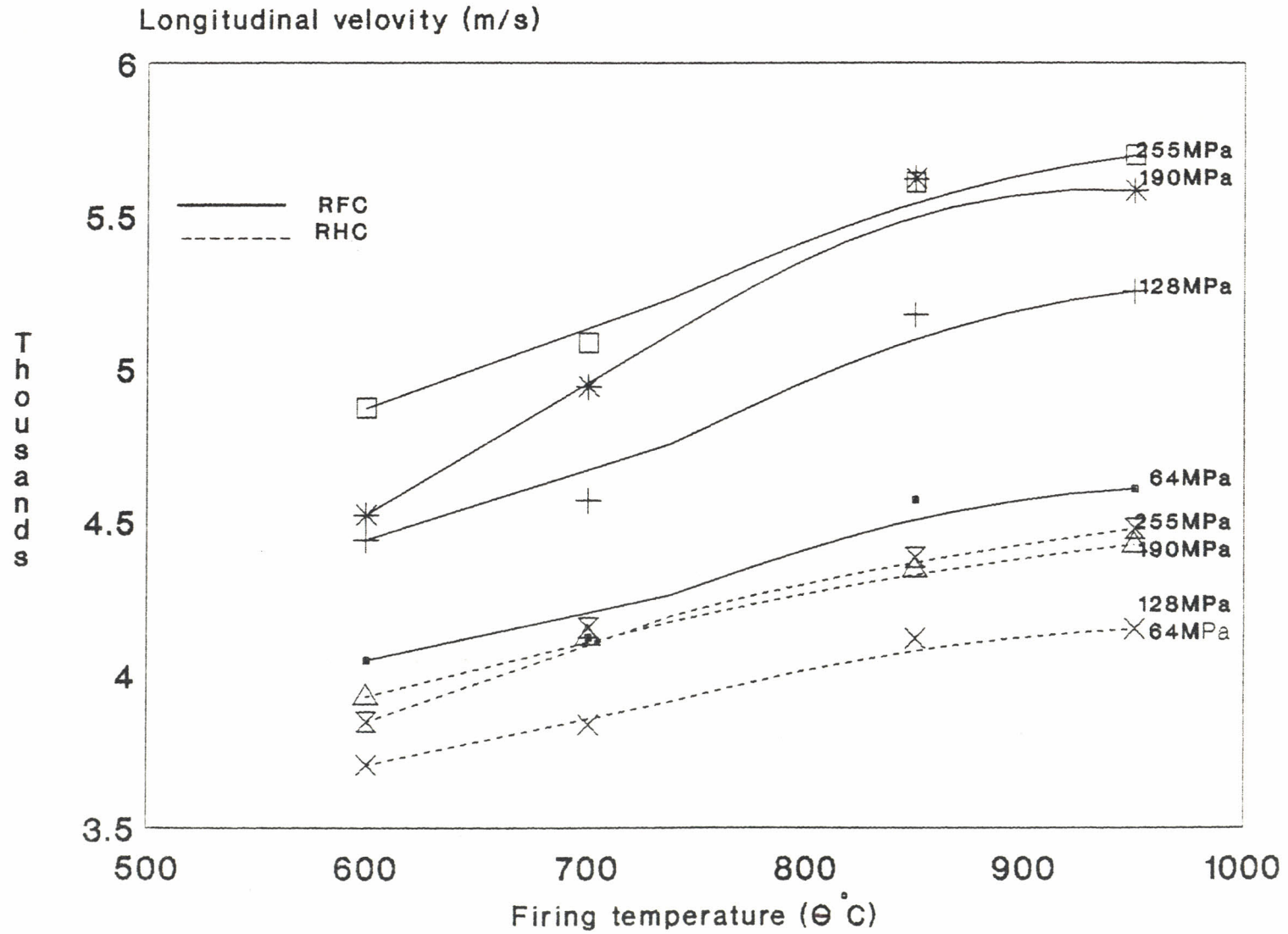
FIG. 5.8

Fig. 5.8 Variation of ultrasonic velocity with temperature

5.7 Modulus of Elasticity (MOE)

The Young's modulus of elasticity was calculated for multiple samples of each clay by substituting $V_1 \cong (2)^{0.5} V_s$ [Gault, 1989] in equation 3.11 i.e

$$E = \frac{\rho V_s^2 \left\{ 3V_1^2 - 4V_s^2 \right\}}{\left\{ V_1^2 - V_s^2 \right\}}$$

this reduces the above equation to

$$E \cong \rho V_1^2 \qquad \dots\dots\dots\dots\dots\dots\dots\dots\dots\dots(5.1)$$

where ρ is the sample density and V_1 is the longitudinal velocity in the sample. In this case the clay samples were assumed to be isotropic. Table 5.8 gives the calculated values of Young's modulus for various sample porosities.

Of the equations that describe the porosity dependence of Young's modulus in brittle solids that were given in Table 2.1, the equations given by Phani et al, (1986) and Wagh et al, (1991) reproduced below were chosen to find the one that best describes the dependence of Young's modulus E on porosity p. These equations are;

$$E = E_o(1 - a\rho)^n \qquad \dots\dots\dots\dots\dots\dots\dots\dots\dots(5.2)$$
$$E = E_o(1 - \rho)^m \qquad \dots\dots\dots\dots\dots\dots\dots\dots\dots(5.3)$$

Equation 5.2 was proposed by Phani et al, while equation 5.3 was given by Wagh et al. In these equations, E and E_o are the Young's modulus at

70

T A B L E 5.8

Calculated log of MOE (E) values for various sample Porosity values

RFC Samples			RHC Samples		
Porosity (p)	Log (1-p)	E (GPa)	Porosity (p)	Log (1-p)	E (GPa)
0.209	0.102	54.99	0.247	0.123	32.87
0.211	0.102	55.96	0.248	0.124	33.82
0.213	0.104	53.50	0.250	0.125	33.13
0.214	0.104	51.30	0.251	0.126	31.76
0.215	0.105	51.35	0.252	0.126	32.78
0.221	0.108	51.50	0.256	0.128	29.47
0.223	0.120	52.02	0.258	0.130	30.73
0.229	0.113	45.34	0.259	0.131	29.52
0.233	0.115	43.44	0.260	0.131	29.18
0.236	0.117	41.23	0.263	0.133	26.25
0.241	0.120	38.33	0.264	0.133	29.88
0.243	0.120	41.51	0.265	0.134	26.89
0.244	0.121	41.44	0.274	0.140	23.52
0.247	0.123	34.72	0.275	0.140	23.76
0.250	0.125	33.63	0.282	0.144	22.70
0.256	0.128	33.47			
0.260	0.131	29.29			
0.272	0.138	28.05			
0.276	0.140	28.20			
0.278	0.141	28.01			
0.279	0.142	25.98			
0.282	0.144	26.09			

porosities p and zero respectively, a, m and n are material constants. `a´ is related to the packing geometry and the pore structure of a material while `n´ and `m´ are dependent on grain morphology and pore geometry of a material. Equation 5.2 shows that E = 0 when $a = 1/p_{crit}$, where p_{crit} is the critical porosity at which E becomes zero. This suggests that a is always greater than 1. Knudsen, (1959) showed theoretically that the value of the packing geometry factor (a) lie in the range $1 \leq a \leq 3.85$ for polycrystalline materials composed of uniform spherical particles arranged in cubic, orthorhombic, or rhombohedral arrays.

Fig. 5.9a and 5.9b show the theoretical and experimental curves for Young´s modulus RFC and RHC samples respectively. The curves shown correspond to equations 5.2 and 5.3. For Equation 5.2, the curves were fitted for the best fits by plotting $\log E$ versus $\log (1 - ap)$ for values of `a´ that maximize the regression coefficient. A commercial software was used for this purpose.

Table 5.8b gives the values of all the parameters corresponding to both equations 5.2 and 5.3. Of the two equations fitted over the entire range of porosity (20.9 - 28.2%), equation 5.2 provided a fit in both RFC and RHC with the minimum standard error of estimate in the theoretical values of E. For this equation the values of E_o obtained in both RFC and RHC were 371.5 GPa and 186.2 GPa respectively. These values of E_o are comparable with those obtained for a wide range of polycrystalline brittle solids [Phani *et al*, 1987]. For both equations, the values of `n´ in both RFC and RHC (Table 5.9) were greater than 2 but lay within the range of ceramics

72

FIG. 5.9a

Young's modulus (GPa)

Legend:
$E = E_o(1-P)^{8.33}$
$E = E_o(1-1.46P)^{4.84}$
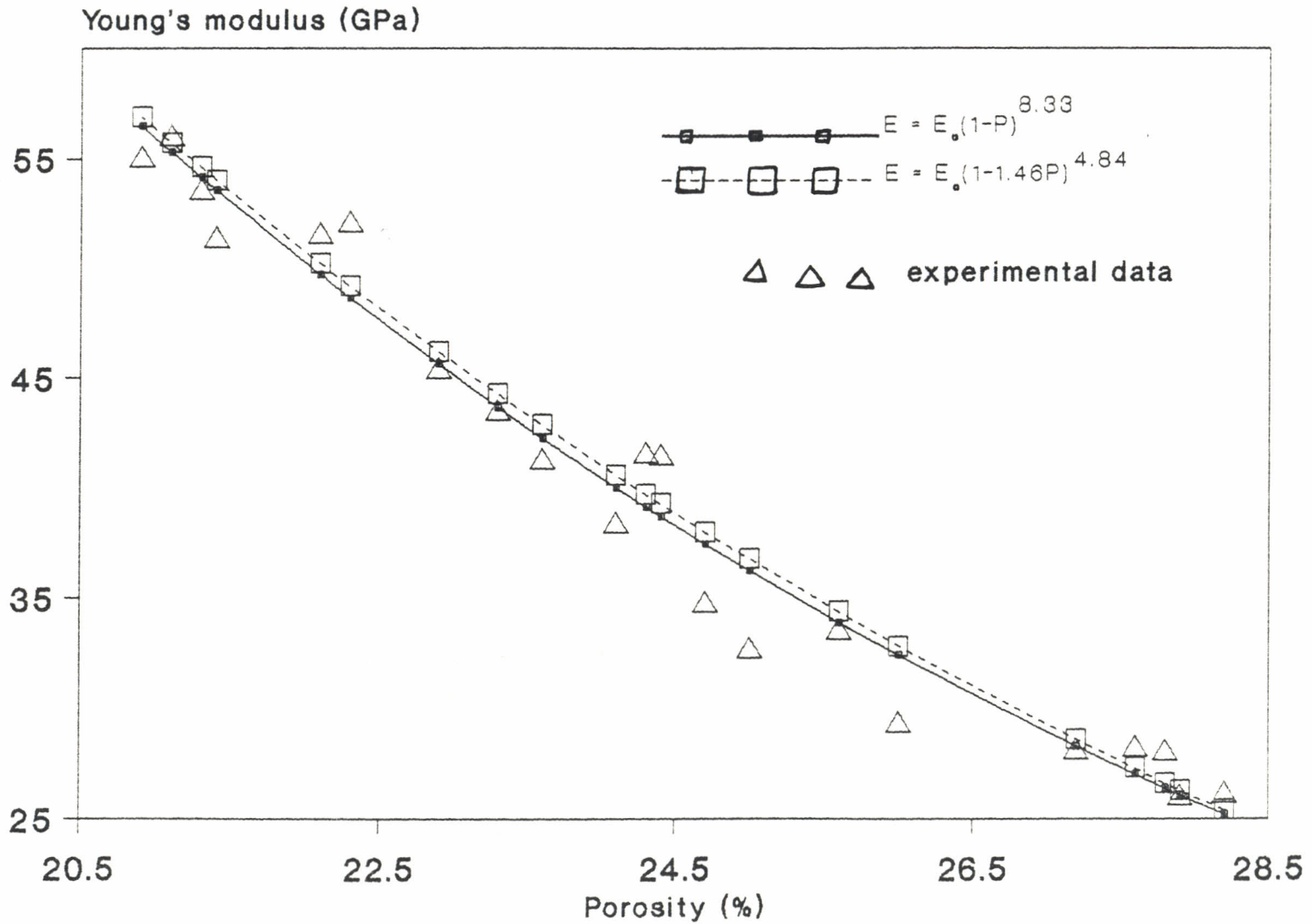△ △ △ experimental data

Porosity (%)

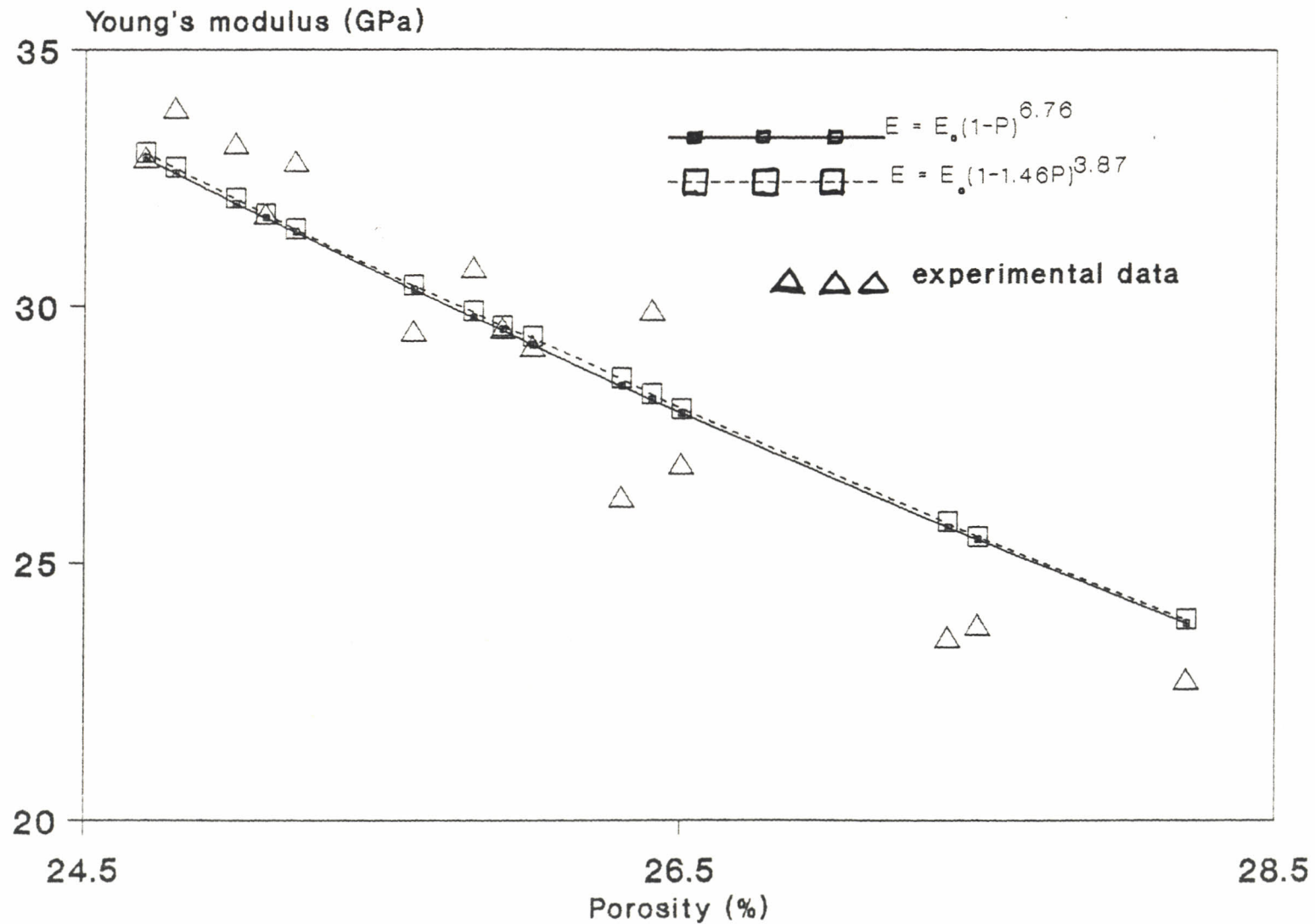Fig. 5.9a - Young's modulus-porosity relationship in RFC

FIG. 5.9b

Fig. 5.9b -Young's modulus-porosity relationship in RHC

given by Phani *et al*, (1987) of 0.65 and 9.57. Comparatively, the lower value of n observed in RHC could be attributed to the wider range of particle size distribution in RHC (Table 5.1) compared to that in RFC. A wide range of particle sizes facilitated better compaction in RHC samples compared to RFC samples which had a `narrower´ range of particle size distribution.

A comparison of `n´ and `m´ values obtained in our study with those obtained for other ceramics [Phani *et al*, 1987; Wagh 1991] indicate that the pores in our samples deviate from spherical shape and might have been interconnected. Most ceramic materials with closed spherical pores and disordered structures (such as α-alumina, sintered glass and some gypsum systems had values of n approximately equal to 2 [Phani *et al*, 1987]. Disordered structures and non-sphericity of pores were possible in our samples since the samples were formed by compaction. Further, photomicrographs (see section 5.9) show such disordered structures in our clay samples.

TABLE 5.9

Summary of parameters of regression lines for Young's modulus of RFC and RHC samples.

Equation	Clay sample	
	RFC	RHC
$E = E_o(1-p)^m$	$E_o = 398.11 \quad m = 8.33$	$E_o = 229.9 \quad m = 6.76$
$E = E_o(1-ap)^n$	$a = 1.46 \quad E_o = 371.54 \quad n = 4.84$	$a = 1.46 \quad E_o = 186.2 \quad n = 3.87$

In summary, it seems that within the porosity range investigated (20.9 - 28.2), both the two equations give nearly the same results.

5.8. Ultrasonic attenuation

The ultrasonic attenuation values at various sample processing conditions are given in Table 5.9. Variations of this parameter with sample density and firing temperature is shown in figures 5.10 and 5.11. respectively. In these figures, it was observed that the ultrasonic attenuation decreases with increasing sample bulk density (Fig. 5.10) and firing temperature (Fig. 5.11). In both types of clay samples, the rate of decrease in attenuation was high at low bulk density values (Fig 5.10) and at low firing temperatures (less than $750^{\circ}C$). Figure 5.12 shows the variation of ultrasonic attenuation with sample porosity. The trend in both clay samples was linear with RHC samples showing a steeper slope compared to RFC samples.

On the average, RHC samples showed high and significant variations of attenuation with sample density within small bulk density and porosity ranges. Further, from Fig. 5.10 and 5.11 it was observed that samples fired at low temperatures were more attenuating compared to those fired at high temperatures. Between the temperature range of $600^{\circ}C$ and $750^{\circ}C$, the rate of decrease in the ultrasonic attenuation was higher than at higher temperatures. As observed earlier (Figs. 5.5 and 5.8), it was within this same temperature range that high rates of increase in bulk density and ultrasonic velocity in the clay samples occurred.

Since the ultrasonic attenuation due to scattering is microstructure dependent (i.e.depends on grain size, shape and size of the pores),it therefore means that during firing, the extent of microstructural changes in a sample determine the amount of attenuation in a sample.

77

For example, photomicrography studies (section 5.9) revealed the growth in size and number of quartz phases with increasing firing temperature. Since large phases provide few scatterers compared to small phases the ultrasonic attenuation in most samples will be expected to decrease with increasing firing temperature (Fig 5.11). Further, during compaction, particle rearrangement in samples with a wider range of particle sizes results in a denser matrix. The measured attenuation in samples with a denser matrix will be observed to decrease more with increasing compaction pressure or density (as seen in RHC samples, Fig 5.10) compared to the attenuation in a less dense sample (i.e RFC samples).

Fig. 5.12 shows that RHC samples were more attenuating at higher porosity values (i.e. greater than 27.0%) compared to RHC samples. This was attributed to the larger size of scatterers (grains) in the RHC samples due to its coarser particle size distribution. Ultrasonic attenuation in the rayleigh scattering regime depends on the cube of the scatterer's diameter. However, at high firing temperatures, RFC samples must have developed larger pores as a result of decomposing organic matter which was observed to be present in RFC samples (Table 5.2b). The overall effect of increased pore sizes in RFC samples on the ultrasonic attenuation may have dominated the attenuation due to larger grains in RHC samples resulting in higher attenuation values at higher temperatures (lower porosities) in RFC samples as observed in Fig. 5.12.

T A B L E 5.10

Measured attenuation in clay samples at various sample processing conditions

Compaction Pressure (± 2.5MPa)	Firing Temp. ($\pm 10^{\circ}$c)	RFC		RHC	
		Average ρ	Average α(db/mm)	Average ρ	Average α(db/mm)
64.0	600.0	1.541	0.572	1.594	0.712
	700.0	1.546	0.440	1.612	0.475
	850.0	1.546	0.275	1.629	0.293
	950.0	1.550	0.180	1.634	0.205
128.0	600.0	1.600	0.435	1.611	0.495
	700.0	1.602	0.285	1.630	0.367
	850.0	1.609	0.172	1.642	0.204
	950.0	1.627	0.120	1.648	0.150
255.0	600.0	1.651	0.300	1.630	0.378
	700.0	1.674	0.220	1.656	0.269
	850.0	1.682	0.140	1.664	0.172
	950.0	1.689	0.110	1.671	0.145

FIG. 5.10
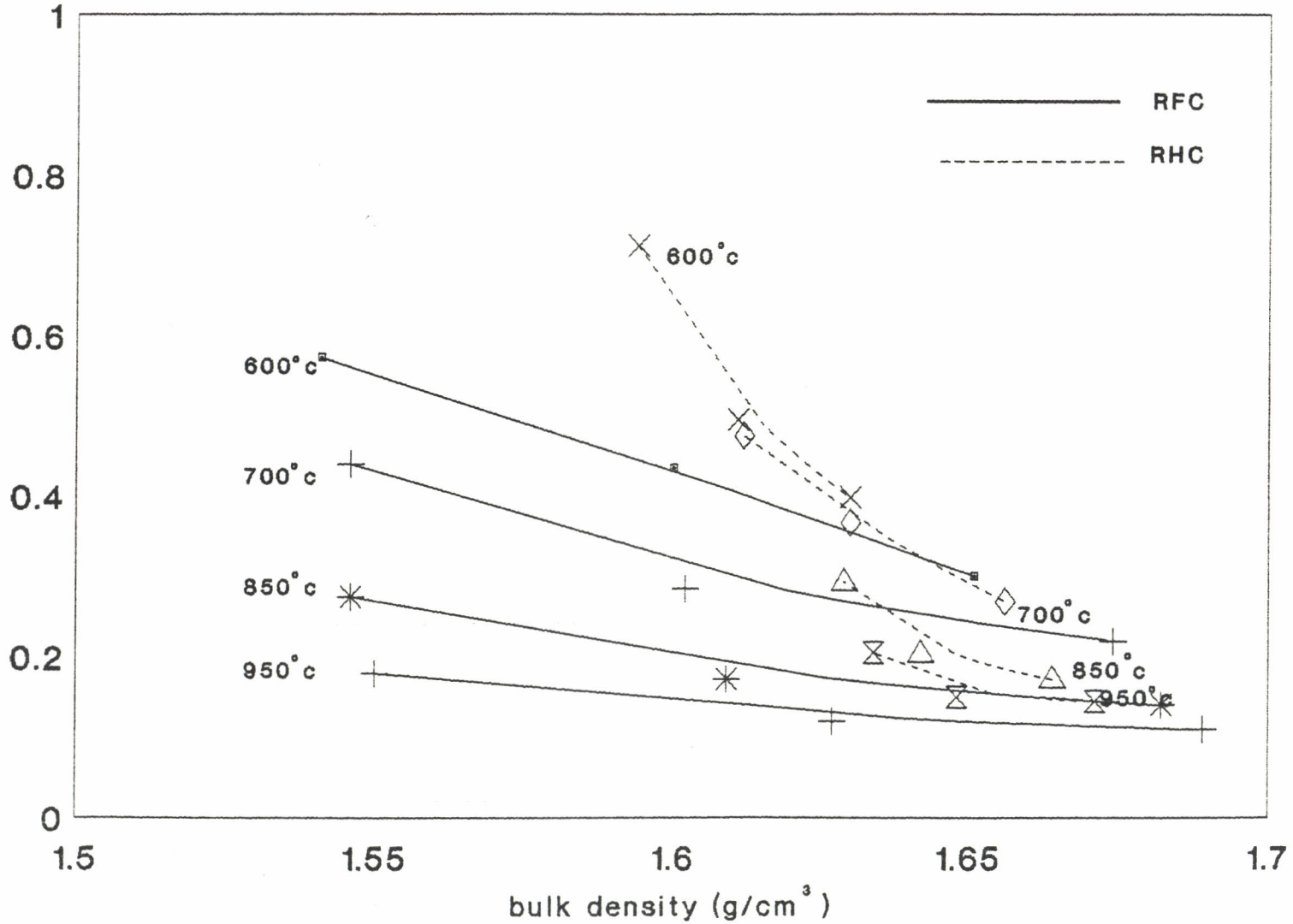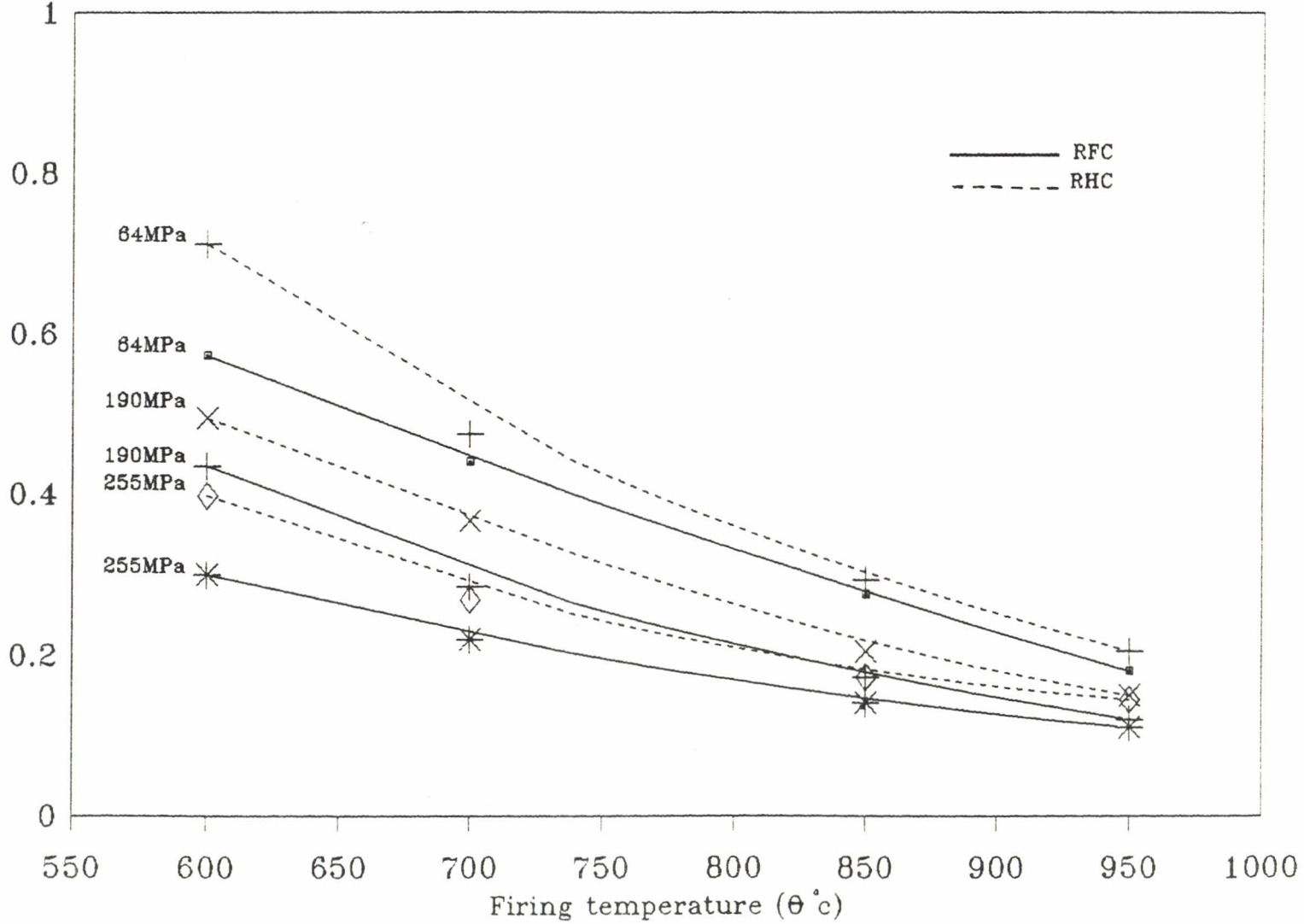
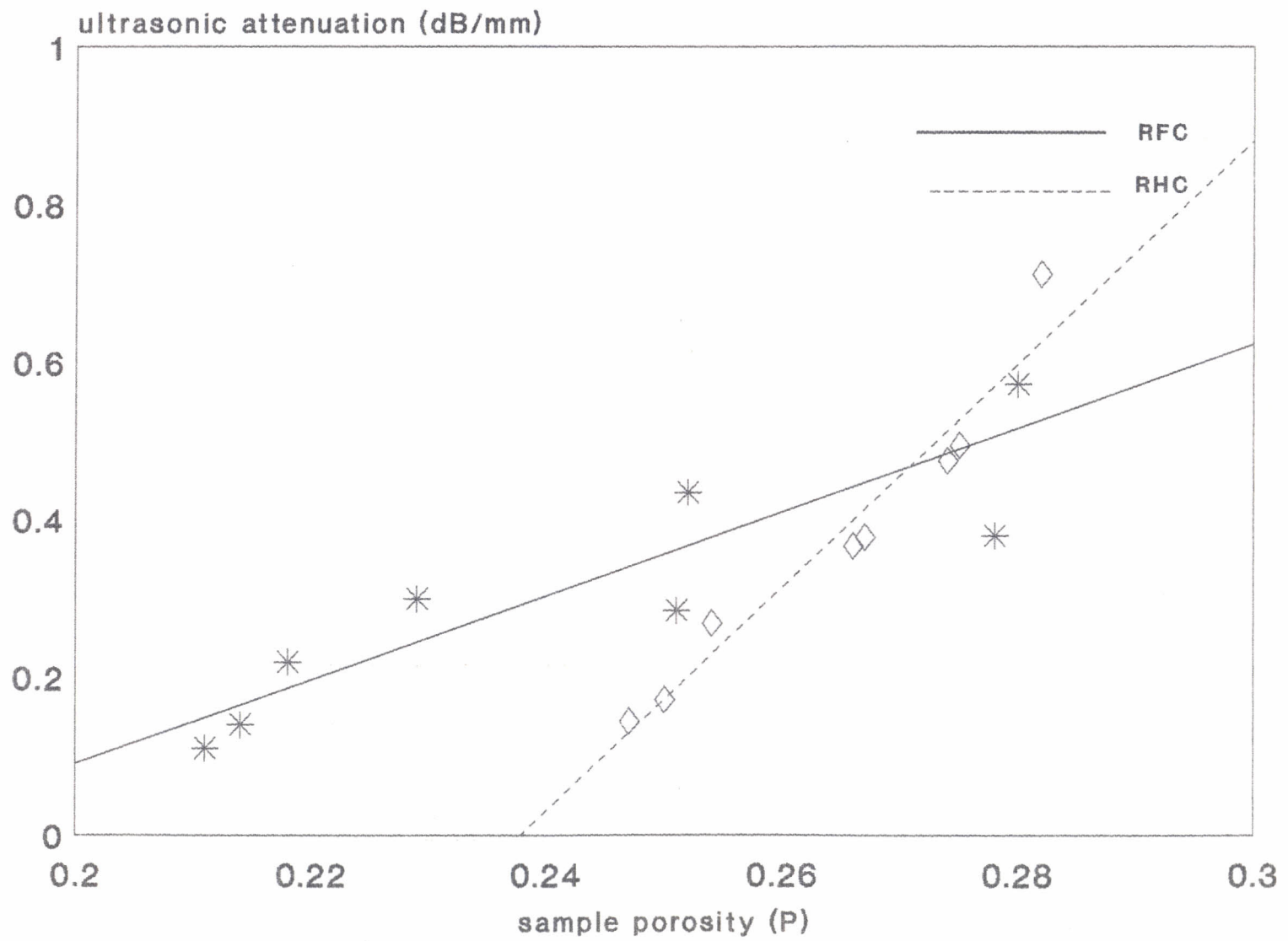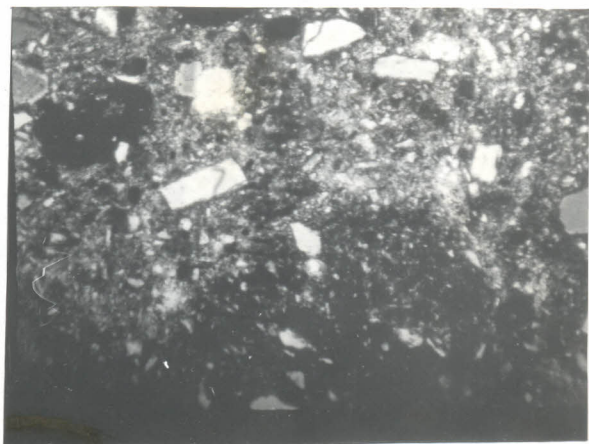Fig.5.10. Attenuation variations with sample bulk density

FIG. 5.11

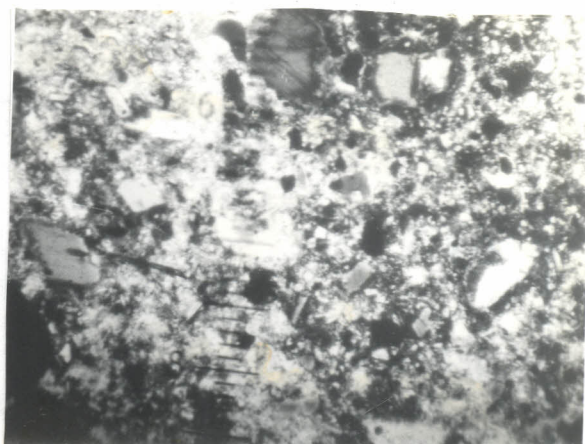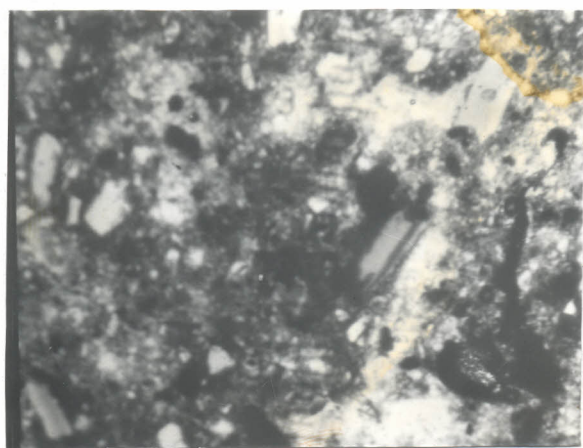Fig. 5.11 –Variation of attenuation with temperature

FIG. 5.12

Fig. 5.12. Ultrasonic attenuation-porosity relationship

(a) -fired at 600°C

(b) -fired at 700°C

(c) -fired at 850°C

(d) -fired at 950°C

Fig. 5.13. -RFC samples compacted at 64 MPa. The white
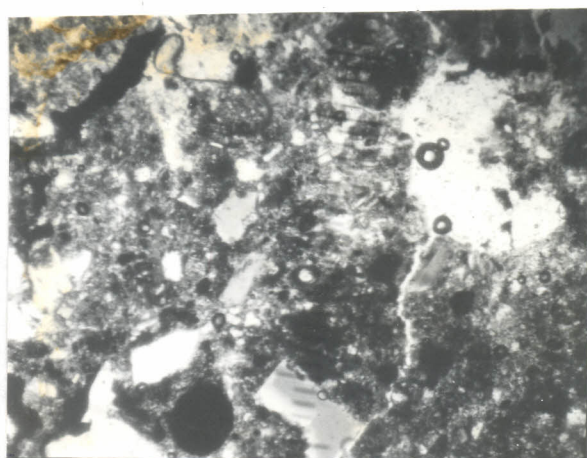phases   are quartz particles.
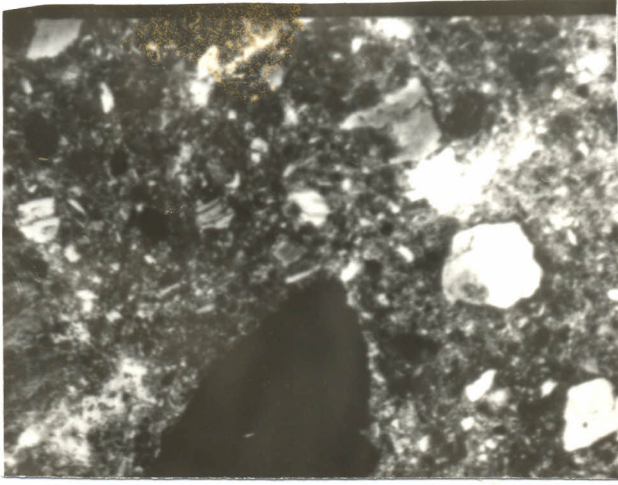
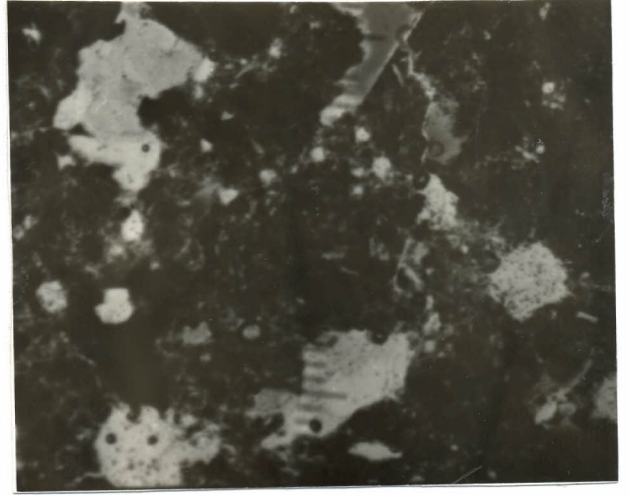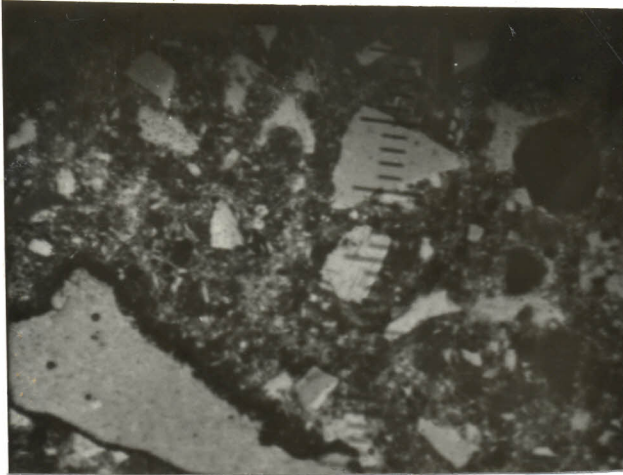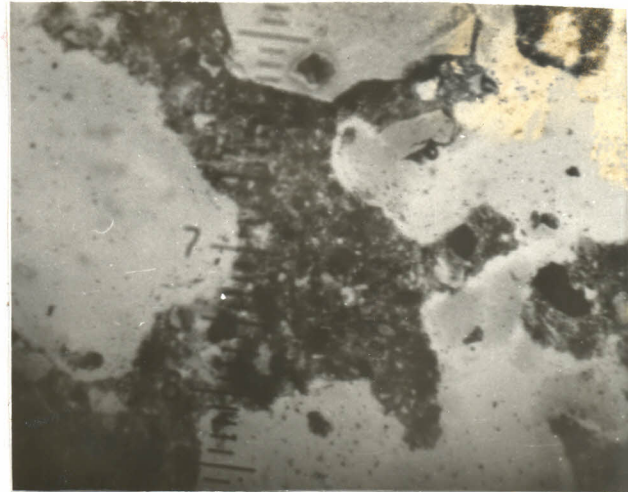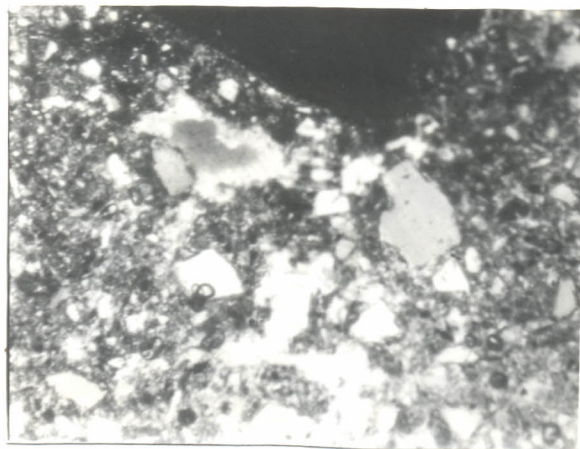(a) -fired at 600°C

(b) -fired at 700°C

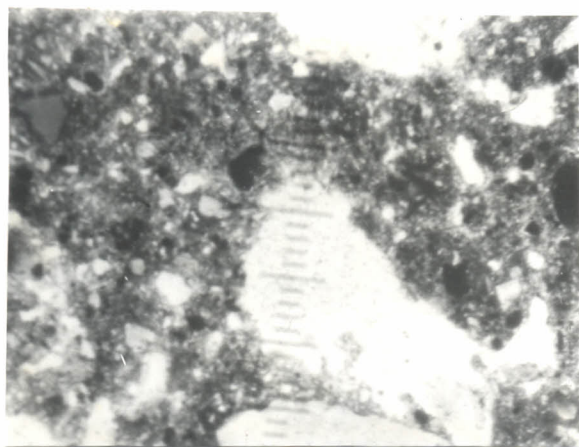
(c) -fired at 850°C

(d) -fired at 950°C

Fig. 5.14. -RHC samples compacted at 64 MPa. The white phases are quartz particles.

(a) -RFC sample fired at 600°C

(b) -RHC sample fired at 600°C

Fig. 5.15. -RFC and RHC samples compacted at 255 MPa and fired at 600°C. The white phases are quartz particles.

5.10   Relations between ultrasonic signals and microstructure.

Photomicrography   studies   have   revealed   that   the   microstructure depends on sample processing conditions such as firing temperature and compaction pressure. The quartz phases were observed to increase in size and number with increasing temperature. Increasing compaction pressure was observed to reduce the distance between the quartz phase centres.

The increase in ultrasonic velocity and the decrease in ultrasonic attenuation with increasing firing temperature and sample bulk density respectively could be attributed to the microstructural changes   that occur on firing such as the change in size of quartz phases and pores. Both pores and quartz phases were observed to influenced   the ultrasonic velocity and attenuation respectively. The very large phases found in samples fired at higher temperatures provided few scatterers compared to the smaller phases that were observed to exist at low firing temperatures. For all phases, Rayleigh scattering regime was still assumed.

In summary, the internal structure of the clay samples influence the propagation of ultrasonic parameters in the samples

C H A P T E R   S I X

CONCLUSIONS AND SUGGESTIONS FOR FURTHER WORK

6.1   Conclusions

The propagation of ultrasonic waves in fired local clay samples has been studied and the effectiveness of the ultrasonic parameters for the nondestructive evaluation of these clay products assessed. It has been shown that the ultrasonic parameters i.e. ultrasonic attenuation and velocity in clay product samples are dependent on sample fabrication conditions (such as compaction pressure and firing temperature).

The fabricating conditions i.e. particle size distribution, firing temperature and compaction pressure were observed to affect the drying shrinkage, firing shrinkage and sample bulk density. High drying and firing shrinkage were observed in samples with a `finer´ particle size distribution, in this case RFC. The bulk density of the samples increased with increasing loading pressures as well as with increasing firing temperature. In both cases, the rate of increase of bulk density was linear at first, followed by a slow down in the rate. The dependence of sample bulk density on compaction pressure and firing temperature showed that not only is the maximum specimen density achieved at high compaction pressures but also at a high firing temperature.

The mineralogical proportions in the samples and the samples microstructure were observed to alter with firing temperature. Quartz phases were observed to increase in size with increasing firing temperature.

88

The variations of the measured longitudinal velocities with firing temperature and compaction pressure were similar to the trend of variation taken by the bulk density with these fabricating parameters respectively. This observation showed that longitudinal velocity in the samples was determined by the samples microstructure via the fabricating conditions. Further, the linear relation between the longitudinal velocity with bulk density shows that not only can the density of a sample be determined from longitudinal velocity measurements, but other microstructural dependent material properties such as elastic moduli can be evaluated from velocity measurements.

The ultrasonic attenuation in the samples was observed to decrease with increasing firing temperature and increasing sample density (decreasing porosity) respectively. This variation was attributed to the microstructural changes associated with firing temperature where by an increase in size of for example, quartz phases and pores was observed. The ultrasonic attenuation can therefore be said to be dependent on the internal structure of the samples.

It is clear that there is a strong dependence of ultrasonic signals on material microstructural details such as the arrangement of particles and particle size distribution. Since the microstructure in the clay samples was found to be dependent on fabricating conditions, it can be concluded that the fabricating conditions affect the ultrasonic signals via the microstructure.

Further, since fabricating conditions especially the firing

temperature and compaction pressure has been found to influence the material properties and the microstructure, controlling fabrication parameters can improve the material properties.

6.2 Suggestions for further work

The present Ultrasonic study was limited to a maximum firing temperature of $950^{O}C$. Extension of this work to higher temperatures will make it possible to determine the optimal firing temperature at which the sample bulk density and the measured ultrasonic velocity attain maximum values.

In the present study only two types of local clays were studied. Extension of this work to other types of local clays is vital. Further, since most ceramic products are fabricated by mixing several types of clays, ultrasonic studies of different compositions of clay mixtures will be helpful in determining the best clay composition for a ceramic ware.

It is hoped that such studies will be useful to our local ceramic industry.

APPENDIX 1

'Rational' and 'Proximate' analysis

The chief minerals present in local clays are kaolinite, micas and quartz. The formula assumed for these minerals, with their respective molecular weight, are shown in Table A below [Worrall 1986].

TABLE A

The chief minerals present in local clays

MINERAL	FORMULA	MOLECULAR WEIGHT
Kaolinite	$Al_2O_3.2SiO_2.2H_2O$	258.17
Soda mica	$Na_2O.3Al_2O_3.6SiO_2.2H_2O$	764.43
Potash mica	$K_2O.3Al_2O_3.6SiO_2.2H_2O$	796.65
Quartz	SiO_2	60.09

To calculate the mineralogical composition in a clay sample from the ultimate chemical analysis (proximate analysis) of Table 5.2a, one has to commence with the alkalis for simplicity. Since the molecular weight of Na_2O is 61.98, it will be seen from Table A that 61.98 parts by weight of Na_2O correspond to 764.43 parts by weight of soda mica, Therefore;

$$1 \text{ part of } Na_2O \equiv 764.43/61.98 \text{ parts of soda mica}$$

$$= 12.33 \text{ parts of soda mica}$$

From Table 5.2a, the percentage of Na_2O in green (unfired) RFC is 0.5, hence the percentage of soda mica is $0.5 \times 12.33 = 6.17\%$

In exactly the same way, it is found that 1 part by weight of K_2O is

equivalent to 8.46 parts of potash mica, and hence the percentage of potash in the clay is 0.7 × 8.46 = 5.92%

To calculate the amount of kaolinite in this sample (green unfired RFC), one has to find the amounts of alumina (total 22.3 from Table 5.2a) contained in potash and soda mica whose amount is known. The calculated percentage of alumina in soda mica is 40.02 % and so the percentage alumina combined as soda mica is 6.17 × 0.4002 = 2.47%. Similarly, the percentage of alumina in potash mica is 38.40% and so the amount of alumina combined as potash mica is 5.92 % × 0.3840 = 2.27 %.

Hence the total alumina in the form of micas = 2.47 + 2.22

= 4.69%.

Therefore, remainder of the alumina (combined in the form of kaolinite) is = 22.30 - 4.69 = 17.61 %. From the molecular weight of Al_2O_3, 101.96 parts of Al_2O_3 correspond to 258.17 parts of kaolinite. Therefore, 1 part of Al_2O_3 correspond to (258.17/101.96) parts of kaolinite

Therefore, 17.61 parts of Al_2O_3 = (258.17/101.96) × 17.61

= 44.59 %

The amount of 'free silica' or quartz is calculated in the same way by first calculating the amount of combined silica (in the same way as for alumina) and then subtracting this amount from the total silica, giving the quartz. In this way the combined silica was found to be 26.25% so that free silica = 65.40 - 26.25 = 39.15%, the percentage of quartz.

The rational analysis results are summarized in Table 5.2b It will be noted in most cases that the totals of major constituents fall short of 100%. The unrepresented percentage is assumed to be miscellaneous oxides and organic matter that are not indicated in the calculation.

LIST OF REFERENCES

Aly Fanzy and C. E. Semler, "Prediction of Refractory Strength Using Nondestructive Sonic Measurements', *American Ceramic Society Bulletin*, **64.** (12). 1555 - 58, (1985).

Addel-aziz A., Khalil, and A.M. Kabesh., `Effect of Sand Particle Size Distribution on the Ceramic Properties of the Fired Clay Bodies'., *Industrial Ceramics* **11(4).**, 188-192, (1991).

Angusto Ib´anez, P. Pena, F. Sandoval, and J. M. Gonz´alez Pena., "Modification of the Inert Component in Wall-Tile Bodies", *American Ceramic Society Bulletin*, **71** (11), 1661-1668, (1992).

Bhardwaj M. C; "Principals and Methods of Ultrasonic Characterization of Materials", *Advanced Ceramic Materials*, **1** (4), 311-324, (1986).

Bilgutay N. M., Li X., and J. Samie., `Spectral Analysis of Randomly Distributed Scatterers for Ultrasonic Grain Size Estimation´, *Ultrasonics* **27** 19-25, (1988).

Blitz J., Elements of Acoustics., Ceramics and Glass. Selected Government Research Reports **10.**, 36-70, (1952).

Choudhury H.S.K.,Materials Science and Processes., J.K. publishers, London, 464 -499.,(1977).

Drury J. C. `Ultrasonic Flaw Detection for Technicians, Inspectorate UK holdings limited, 9-52,. (1987).

El G. and S. Baste, `Evaluation of Anisotropic Damage in Ceramic —Ceramic (SiC-SiC) Composite by Ultrasonic Method.´ *Ultrasonics International 89 Conference Proceedings*, 895-900, (1989).

Evans A.G., B.R. Tittman and L.Ahlberg, "*Ultrasonic Attenuation in Ceramics*" J. Appl. Phys, **45.** (5), 2669-2679., (1978).

Frederick J.R.,"Ultrasonic Engineering" John Wiley and Sons, Inc. NY., 1965.

Fu, L. S., "On the Feasibility of Quantitative Ultrasonic Determination of Fracture Toughness" - A literaure review in *International Advances in Non-destructive Testings*, Gordon and Breach., 8., 87 - 116, (1981).

Gault C., `Ultrasonic Nondestructive Evaluation of Microstructural Changes and Degradation of Ceramics at High Temperatures.´, *Mat. Res. Soc. Symp. Proc.* 142., 263-274., (1989).

Gaydecki P.A., F.M. Burdekin, W. Damaj., D.G. John and P.A. Payne. "The Propagation and Attenuation of Medium-frequency Ultrasonic Waves in Concrete; A Signal Analytical Approach"., Meas. Sci. Technol. 3., 126-134, (1992).

Gieske, H., and F. M. Harold, `Technique for Measuring Ultrasonic Velocity and Attenuation Changes in Attenuative Materials at Temperatures Such as During Sintering Processes´., *Rev. Sci. instrum.* 62 (12), 3056-3060., (1991).

Hefetz, M. and S. I. Rokhlin, `Thermal Shock Damage Assessment in Ceramic Using Ultrasonic Waves´, *J. Am. Ceram. Soc.* 75 (7), 1839-45., (1992).

Ibisi M.I., `The Firing Behaviour of Some Nigerian Clays´. *Industrial Ceramic* 11 .(4), 183-186., (1991).

Jones M.P., G.V. Blessing and C. R. Robbins. "Dry- coupling Ultrasonic Elasticity Measurements of Sintered Ceramics and Their Green States"., *Materials Evaluation* 44. (6), 859-862., (1986).

Jones J.J. and M.F. Bernard, `Ceramics Industrial Processing and Testing, The IOWA State University Press., AMES, IOWA,. 2-19., (1972).

95

Kathrina, T., R. Round and B. Bridge, `An Investigation of the Composition Dependence of the Elasticity, Reaction Rate and Porosity of Orthophosphate Bonded Ceramics Using the Ultrasonic Double-probe Method", *J. Phy. D: App Phy.*, 24 ., 1673 - 1686, (1991).

Kendall K. `Ultrasonic Studies of Ceramic Powders During Compaction´, *Brit. Ceram., Trans.* 89, 211-213, (1990).

Kingery W.D. Introduction To Ceramics ., John Wiley and Sons, Inc., NY., 33-77., (1975).

Knudsen F. P., `Dependence of mechanical strength of brittle polycrystalline specimens on porosity and grain size´, *J. Am. Ceram., Soc.*, 42, (8)., 366-387, (1959).

Klima J.S. and G. Y. Baaklini, "Ultrasonic Characterization of Structural Ceramics" in `Materials Analysis by Ultrasonics by Alex Vary, Noyes Data Corporation, 113-121., (1987).

Kobayashi Y., O. Osamu, Y. Ohashi, and E. Kato., `Effect of Firing Temperature on the Bending Strength of Porcelains For Tableware´, J. *Am. Ceram., Soc.*, 75. (7)., 1801-1806, (1992).

Kreher W., Ranachowski J. and F. Rejmund, `Ultrasonic Waves in a Porous Ceramic with Non-spherical Holes.´, Ultrasonics, 70-73., (1977)

Kunerth D. C., Telschow K.L. and Waller J. B., `Characterization of Porosity Distribution in Advanced Ceramics; A comparison of Ultrasonic Methods´, *Materials Evaluation*, 47(5), 571-574, (1989).

Kupperman D. and H. B. Karplus. "Ultrasonic Wave Propagation Characteristics of Green Ceramics.´, *Ceramic Bulletin.* 63 (12)., 1505-1509, (1984).

Kshama V. D., Mohan B. V., and Lilithambika M., `Sintering Studies On Plastic Clays´, Ceramic International 18, 359-364, (1992).

Lefebvre J., Frohly J., R. Torguet, C. Bruneel, and J.M. Rouvaen., "Experimental and Theoretical Study of the Multiple Scattering of Acoustic Waves in Inhomogeneous Media "., *Ultrasonics*, 170-174, (1980).

Mittleman and David W. W., `Correlating Microstructure with Backscattered Ultrasonic Energy´., *Mat. Res. Soc. Symp. Proc.* 142. 357-364, (1989).

Nagarajan A. "Ultrasonic Study of Elasticity-Porosity Relationship in Polycrystalline alumina´,*Journal of Applied physics.*, **42** (10)., 3693 – 3697, (1971).

Nosbusch H. and I.V. Mitchell, `Clay-Based Materials for the Ceramic Industry, John Wiley and sons, Inc., N.Y., 93-100., [1986].

Orenstein R. M., and David J. G., `Thermal Shock Behaviour of Open -cell Ceramic Forms´, *J. Am. Ceram. Soc.*, **75** (7)., 1899-1905, (1992).

Ranachowski J., `Propagation of Ultrasonic Waves in Porous Ceramics´, *Ultrasonics*, 203-207, (1975).

Panakkal J. P., `Use of Longitudinal Ultrasonic Velocity as a Predictor of Elastic Modului and Density of Sintered Uranium Dioxide´. *IEEE., Transactions on Ultrasonics, Ferroelectrics and Frequency Control.*, **38** (3)., 161-165, (1991).

Phani K. K.,"Youngs Modulus-Porosity Relation in Gypsum Systems", *Am. Ceramic. Soc. Bull.*, **65** (12). 1584 – 86, (1986).

Rokhlin S.I., Bolland T.K., and L. Adler, "High Frequency Ultrasonic Wave Propagation in Polycrystalline Materials." *J. Acoust. Soc. Am.* **91** (1), 151-165, (1992).

Serabian S., `Ultrasonic Material Property Determination´ in *Materials Analysis by Ultrasonics* by A. Vary., Noyes Data Corporation., 210-216., (1987).

Serabian S., `Implications of the Attenuation Produced Pulse Distortion Upon The Ultrasonic Method of Non-destructive Testing`., *Material Evaluation*, 173-179, (1968).

Smith R. L. "The Effect of Grain Size Distribution on the Frequency Dependence of the Ultrasonic Attenuation in Polycrystalline Materials", Ultrasonics ., **20** (**5**), 211-214,(1982).

Stepisnik S., and Nankocuvan, "Measurement of Cement Hydration by Ultrasonics". *Ceramic bull.*, 60 (4)., 481-483, (1981).

Stewart G.H. <u>Science of Ceramics Vol.1.</u>, Academic-press London and New York, 1-19., (1962).

Szilard J., `<u>Ultrasonic Testing (Non-conventional Testing Technique)</u>. A John Wiley-Interscience Publication., NY. 1-23., (1982).

Vary A., `Ultrasonic Measurement of Mechanical Properties`., NASA, 44135, Cleveland, Ohio., 1-38, (1988).

Vary A., and Harnold E. K., `Transfer Function Concept for Ultrasonic Characterization of Material Microstructure., NASA. TM. 86880, 940-978., (1985).

Veniale F. `Ceramic Applications of Clays and Clay Minerals State-of-the-art and Perspectives., Industrial Ceramic **12** (**3** ., 105-109., (1992).

Wagh A.S., R.B. Poepplel, J.P. sigh. "Open Pore Description of Mechanical Properties of Ceramics`., J. *Mat. Sci.* **26**., 3862 - 3868, (1991).

Waiser M. W. and Lutgard C. De Jonche. `Rearrangement During Sintering in Two-dimensional Arrays`. *J. Am. Ceram. Soc.*, **69** (11)., 822-26, (1986).

Wear K.A., Wagner, R. F., Michael F. Insana and Timothy J. Hall. `Application of Antoregressive Spectral Analysis to Cepstral Estimation on Mean Scatter Spacing`, IEEE *Transactions on Ultrasonics, Ferroelectrics, and Frequency Control.*, **40** (1), 50-57, (1991).

Worrall W. E., Clays and Ceramic Raw Materials., Elsevier Applied Science Publishers., 177-201, (1986).

Yuidi K., Osamu O., Yasuo O., and E.Kato, "Effect of Firing Temperat - - ure on Bending Strength of Porcelains for Tableware"., J. Am. Ceram. Soc. **75** (7), 1801-1806, (1992).